Geosci. Model Dev. Discuss., 3, 1359–1421, 2010
www.geosci-model-dev-discuss.net/3/1359/2010/
doi:10.5194/gmdd-3-1359-2010
© Author(s) 2010. CC Attribution 3.0 License.

Geoscientific Model Development Discussions

This discussion paper is/has been under review for the journal Geoscientific Model Development (GMD). Please refer to the corresponding final paper in GMD if available.

The global middle-atmosphere aerosol model MAECHAM5-SAM2: comparison with satellite and in-situ observations

R. Hommel[1,*], **C. Timmreck**[1], **and H. F. Graf**[2]

[1]Max Planck Institute für Meteorologie, Hamburg, Germany
[2]Centre for Atmospheric Science, Department of Geography, Cambridge University, Cambridge, UK
[*]now at: Centre for Atmospheric Science, Department of Chemistry, Cambridge University, Cambridge, UK

Received: 22 July 2010 – Accepted: 16 August 2010 – Published: 1 September 2010

Correspondence to: R. Hommel (rene.hommel@atm.ch.cam.ac.uk)

Published by Copernicus Publications on behalf of the European Geosciences Union.

Abstract

In this paper we investigate results from a middle-atmosphere aerosol-climate model which has been developed to study the evolution of stratospheric aerosols. Here we focus on the stratospheric background period and evaluate several key quantities of the global dispersion of stratospheric aerosols and their precursors with observations and other model studies. It is shown that the model fairly well reproduces in situ observations of the aerosol size and number concentrations in the upper troposphere and lower stratosphere (UT/LS). Compared to measurements from the limb-sounding SAGE II satellite instrument, modelled integrated aerosol quantities are more biased the lower the moment of the aerosol population. Both findings are consistent with earlier work analysing the quality of SAGE II retrieved e.g. aerosol surface area densities from the volcanically unperturbed stratosphere (SPARC/ASAP, 2006; Thomason et al., 2008; Wurl et al., 2010).

The model suggests that new particles are formed over large areas of the LS, albeit nucleation rates in the upper troposphere are at least one order of magnitude larger than those in the stratosphere. Hence, we suggest that both tropospheric sulphate aerosols and particles formed in situ in the LS are maintaining the stability of the stratospheric aerosol layer also in the absence of direct stratospheric emissions from volcanoes. Particle size distributions are clearly bimodal, except in the upper branches of the stratospheric aerosol layer where aerosols evaporate. Modelled concentrations of condensation nuclei (CN) are lesser than measured in regions of the aerosol layer where aerosol mixing ratios are largest, due to an overpredicted particle growth by coagulation.

Transport regimes of tropical stratospheric aerosol have been identified from modelled aerosol mixing ratios and correspond to those deduced from satellite extinction measurements. We found that convective updraft in the Asian Monsoon region significantly contributes to both stratospheric aerosol load and size. The timing of formation and descend of layers of fine mode particles in the winter and spring polar stratosphere

GMDD
3, 1359–1421, 2010

(CN layer) are reproduced by the model. Far above the tropopause where nucleation is inhibited due to with height increasing stratospheric temperatures, planetary wave mixing transports significant amounts of fine mode particles from the polar stratosphere to mid-latitudes. In those regions enhanced condensation rates of sulphuric acid vapour counteracts the evaporation of aerosols, hence prolonging the aerosol lifetime in the upper branches of the stratospheric aerosol layer.

Measurements of the aerosol precursors SO_2 and sulphuric acid vapour are fairly well reproduced by the model throughout the stratosphere.

1 Introduction

It has long been recognised that aerosols are an important constituent of the chemical composition of the stratosphere (SPARC/ASAP, 2006; IPCC, 2007). Observations showed that hydrophilic (soluble) sulphate droplets are the major constituent of the particulate matter above the tropopause albeit nitric acid, organics, or meteor debris influence their composition on synoptic scales (e.g. Sheridan et al., 1994; Deshler et al., 2003b; Gerding et al., 2003; Baumgardner et al., 2004; Froyd et al., 2009). Stratospheric aerosols alter the Earth' climate by scattering incoming solar radiation (Lacis et al., 1992), thereby serving as a climate cooling agent (IPCC, 2007). They interact with catalytic cycles of stratospheric ozone depletion by providing surfaces for heterogeneous reactions (e.g. Angell et al., 1985; Borrmann et al., 1997) and play a role in the formation of polar stratospheric clouds and cirrus clouds (Tolbert, 1994; DeMott et al., 2003). Stratospheric aerosol climate interactions become obvious when violent volcanic eruptions emit large amounts of aerosol precursors directly into the stratosphere (reviewed in Robock, 2000). In recent years much attention was paid to ideas to counteract human-induced global warming due to greenhouse gases and to mitigate climate change by means of an artificially increased stratospheric albedo (e.g. Crutzen, 2006; Rasch et al., 2008; Heckendorn et al., 2009).

GMDD
3, 1359–1421, 2010

However, the climate response to stratospheric aerosols is not yet well understood. Model studies of climate impacts from tropical volcanic eruptions with stratospheric injection heights largely disagree in the dynamical responses of the climate system, e.g. in the strengthening of the positive phase of the Northern Atlantic Oscillation and the associated "winter warming" phenomenon as observed after the eruptions of Mt. Pinatubo or El Chichón (Stenchikov et al., 2002, 2006). Also responses of the stratosphere, e.g. positive temperature anomalies at the equator, are not very well captured by models (Thomas et al., 2009). Model studies of the climate impacts and the dynamics of aerosols in the stratosphere which is not perturbed by volcanic material, also referenced as the background state of the stratosphere, significantly differ in the reproduction of aerosol key quantities. While model estimates of the total sulphur load of the stratosphere are in good agreement between models and observations (Kent and McCormick, 1984; Pitari et al., 2002; Takigawa et al., 2002), as shown later, conversion rates of microphysical and chemical processes with respect to stratospheric aerosol formation and depletion significantly differ between the models. The same is true for aerosol transport cycles which are associated with the models ability to reproduce main features of the atmospheric circulation (convective updraft, stratosphere-tropopause exchange, the Brewer-Dobson circulation, and the quasi-biennial oscillation in the equatorial stratosphere) because transport processes to a large degree determine the life cycle of stratospheric aerosols (Trepte and Hitchman, 1992; Hitchman et al., 1994; Holton et al., 1995; Hamill et al., 1997). Deficits are also seen in the model's reproduction of observed aerosol precursor abundances (Mills et al., 2005a; SPARC/ASAP, 2006), although the data base for these measurements is distinctly smaller than that for tropospheric observations (reviewed in SPARC/ASAP, 2006). Furthermore, the relevance of certain processes stabilising the stratospheric aerosol layer also in volcanically quiescent periods, e.g. the partitioning between SO_2 and gaseous H_2SO_4 in altitudes well above the aerosol layer, remains uncertain (Rinsland et al., 1995; Vaida et al., 2003; Mills et al., 2005a,b).

GMDD
3, 1359–1421, 2010

While during volcanically active episodes observations of stratospheric aerosol load, particle size, and effects on the surface climate associated with the stratospheric veil of aerosol largely agree, during volcanically quiescent periods a distinct inconsistency prevails in particular regarding the aerosol size and number (Russell et al., 1996; Deshler et al., 2003a; SPARC/ASAP, 2006; Wurl et al., 2010). Background aerosols are significantly smaller (distribution median radius <0.2 µm) than in a volcanically perturbed stratosphere (distribution median radius >0.4 µm) and the particles' scattering efficiency of incoming solar radiation is reduced. Therefore remote sensing instruments suffer from low-signal-to-noise ratios for the detection of small mode aerosols. In situ instruments measure the number of neutral stratospheric aerosols down to 0.01 µm with adequate accuracy (Deshler et al., 2003a). The measurement uncertainties in the determination of the particle size are approximately ±10% (Deshler et al., 2003a). Remote sensing instruments are practically unable to measure particles of that size. The relative detection error exponentially increases for particles smaller than 0.1 µm in radius (e.g. Dubovik et al., 2000); 0.05 µm sized aerosol measurements yield a relative error of approximately 50%.

To better assess climate relevant processes attributed to stratospheric aerosols by means of global climate models, it is necessary to accurately simulate the dynamics of stratospheric aerosols. This comprises modelling the formation and global dispersion of stratospheric aerosols with simultaneous consideration of various tropospheric processes, since soluble aerosol above the tropopause originates in one form or another from sources in the troposphere (SPARC/ASAP, 2006). Of particular importance for modelling aerosol-climate interactions is the prognostic treatment of the particle size (e.g. Adams and Seinfeld, 2002; Zhang et al., 2002; Dusek et al., 2006). It has been shown that prescribing the size of aerosols in models predicting aerosols as a bulk (e.g. Takigawa et al., 2002; Rasch et al., 2008) instead of interactively predicting the shape of the size distribution (e.g. Timmreck, 2001; Adams and Seinfeld, 2002; Spracklen et al., 2005; Stier et al., 2005) systematically affects model predictions of aerosol and precursor transport and mixing as well as the interaction with chemical cycles in the

GMDD
3, 1359–1421, 2010

atmosphere, and aerosol direct and indirect radiative forcing (e.g. Zhang et al., 2002; Myhre et al., 2004; Heckendorn et al., 2009). Pan et al. (1998) showed that uncertainties in the prediction of the size of sulphates is one of the largest contributors to the general model uncertainty.

Although the integration of comprehensive and interactive aerosol modules in fourth- and fifth-generation climate models significantly improved the understanding of complex climate influences of anthropogenic and natural aerosol (IPCC, 2007; Ghan and Schwartz, 2007), most of the models do not explicitly consider the formation and evolution of aerosols in the stratosphere. Instead, stratospheric aerosol processes are highly simplified. Direct effects of aerosol particles in the stratosphere are quantified from prescribed 3-D climatologies of integrated aerosol quantities, either treated offline from simulations with other models or derived from observations. Only a few models were developed which predict stratospheric aerosol interactively. Due to computational expenses particularly implied by the increase of the vertical resolution in those models, aerosol processes were constrained to bulk descriptions of the aerosol mass (e.g. Timmreck et al., 1999; Takigawa et al., 2002; Rasch et al., 2008). Size resolving aerosol schemes were utilised in the climate model studies of Timmreck (2001) and Pitari et al. (2002) investigating the dynamics of stratospheric background aerosol. The top of the atmosphere (TOA) at 10 hPa (~33 km) in the model of Timmreck (2001) yields differences to observations of meridional aerosol transport and associated effects. However, this model adequately reproduces the global dispersion of stratospheric aerosols. Hence, aerosol key quantities (surface area, effective radius) and aerosol size distributions in the northern hemisphere were in good agreement to observations. The model of Pitari et al. (2002) had a TOA at 0.04 hPa (~72 km) and was interactively coupled to a chemistry model. Apart from reproducing the stratospheric aerosol layer, it successfully reproduced distinct features of the stratospheric composition, e.g. the formation of an Antarctic ozone hole.

There exist few other size resolved aerosol codes coupled to one or 2-D middle-atmosphere dynamics models (Turco et al., 1979; Bekki and Pyle, 1992; Weisenstein

GMDD
3, 1359–1421, 2010

et al., 1997). Some of them are interactively coupled to comprehensive chemistry schemes (Mills et al., 1999, 2005a,b). An inter-comparison of these and the 3-D models of Timmreck (2001) and Pitari et al. (2002) is found in the WMO/SPARC Assessment of Stratospheric Aerosol Properties (SPARC/ASAP, 2006). The report revealed large differences in the model representation of stratospheric aerosols and their precursors and demonstrated that reproducing observations of UT/LS aerosols in the volcanically perturbed as well as the background stratosphere strongly depends on comprehensively resolved transport processes in the models, taking also into account tropospheric processes.

In this paper we evaluate a 3-D model that has been developed to study the dynamics of stratospheric aerosols in volcanically quiescent periods. The model deploys schemes for aerosol microphysics and sulphate chemistry to address the evolution of sulphate aerosols throughout the troposphere and stratosphere. Aerosols are size resolved and prognostic up to the TOA at 0.01 hPa (~80 km). We compare several key quantities of the modelled aerosol layer with observations from the spaceborne SAGE II instrument, in situ measurements made in the northern hemispheric midlatitudes, and data from other models. An essential role is given to the evaluation of aerosol precursor abundances. The model evaluation will address the inconsistency found in integrated aerosol size quantities retrieved from SAGE II and in situ observations, which was recently highlighted in the WMO/SPARC Assessment of Stratospheric Aerosol Properties (SPARC/ASAP, 2006).

In Sect. 2 model and experimental setups are described. In Sect. 3 we evaluate the model by diagnosing the sulphur budget, comparing precursors to published data from literature and observations. We validate integrated aerosol size parameters with two independent SAGE II climatologies based upon different retrieval algorithms. Finally we compare size distributions predicted by the model to in situ measured number densities in the midlatitudes of the northern hemisphere. A summary is given in Sect. 4. The interannual variability of the modelled stratospheric aerosol layer is subject for further analysis in a companion paper.

GMDD
3, 1359–1421, 2010

2 Methods

2.1 Host model

In this work, the aerosol-microphysical module SAM2 is implemented in the middle-atmosphere (MA) configuration of the atmospheric general circulation model (AGCM) ECHAM5. This AGCM was evaluated in several configurations[1]. A detailed description of principal components is found in (Roeckner et al., 2003). The middle-atmosphere configuration MAECHAM5 has a vertical representation of the atmosphere up to 0.01 hPa (~80 km) and comprises a parametrisation of the momentum flux deposition from vertically propagating gravity waves of tropospheric origin after Hines (1997). Details on the model configuration are given in Manzini et al. (2006). In the vertical, the model has 39 σ-hybrid layers. The layer thickness in the UT/LS is ~1.5 km, further expanding to ~2.5 km towards the top of the atmosphere. Prognostic variables are integrated with a spectral triangular truncation at wave number 42 (T42). Corresponding Gaussian grid cells, in which physical processes and non-linear terms are calculated, have a width of ~2.8°×2.8°. The integration time step length is 15 min. As lower boundary conditions we are using climatological mean AMIP2 sea surface temperatures and sea ice concentrations. Prognostic aerosols are decoupled from the ECHAM5 radiation code (Fouquart and Bonnel, 1980; Mlawer et al., 1997), radiative transfer calculations were made every two hours, applying the Tanre et al. (1984) aerosol climatology. Prognostic chemical compounds are advected on a Gaussian grid every time step by applying a semi-Lagrangian transport scheme following Lin and Rood (1996).

[1]See Special Section: Climate models at the Max Planck Institute for Meteorology (MPI-M), Journal of Climate, 19(16), 3769-3987, 2006.

GMDD
3, 1359–1421, 2010

2.2 Aerosol module

The aerosol microphysics module SAM2 is based on the size-segregated aerosol module SAM of Timmreck and Graf (2000). In its new formulation the module is not restricted to the stratosphere – it treats the formation and evolution of sulphuric acid-water (H_2SO_4/H_2O) aerosol droplets throughout the atmosphere. The module considers the aerosol microphysical processes of binary homogenous nucleation, condensation and evaporation of sulphuric acid and water, as well as particle coagulation. The sulphuric acid droplets are assumed to be spherical and in thermodynamic equilibrium with the environment, which is a valid assumption at the time scales of interest (Hamill et al., 1977; Steele and Hamill, 1981). Details on the thermodynamic parametrisations are given in Timmreck and Graf (2000). Following the fixed sectional approach (e.g. Gelbard et al., 1980), the scheme resolves the aerosol size from 1×10^{-3} µm to ~2.6 µm in 35 logarithmically spaced bins which are determined by mass doubling. The interaction between aerosols and processes affecting the Earth' climate depends for several reasons on the size of aerosols. To assess size dependent aerosol properties, it makes sense to divide an aerosol population into subranges, independent on the numerical discretisation of the aerosols size spectrum. For diagnostic purposes the following subranges are defined: a nucleation mode where aerosols have radii R_p smaller than <0.005 µm, an Aitken mode (0.005 µm $\leq R_p <$ 0.05 µm), an accumulation mode (0.05 µm $\leq R_p <$ 0.5 µm) and a coarse mode ($R_p \geq$ 0.5 µm).

In preceding studies of Timmreck (2001) on the evolution of stratospheric background aerosols, by using the predecessor module SAM coupled to an AGCM with a top of the atmosphere at ~30 km, only the total mass of aerosols was prognostic (bulk approach). In the new version introduced here each of the discretised aerosol size sections is prognostic and advected as an atmospheric tracer.

The operator splitting technique is used to integrate the aerosol dynamic equation (Seinfeld and Pandis, 1998). New particle formation via binary homogeneous nucleation and the density of the binary mixture H_2SO_4/H_2O are parametrised after

GMDD
3, 1359–1421, 2010

Vehkamäki et al. (2002). The number of particle nuclei with a size smaller than the module's lower threshold size is scaled into the smallest defined size class, thereby preserving the net sulphur concentration.

The condensation of H_2SO_4 onto aerosols as well as their partial evaporation are number conserving processes. To preserve aerosol number we applied a 1-D hybrid exponential-upwind advection scheme which allows aerosols to change their size in radius space. Mass is conserved via a serial operating, non-iterative algorithm that traces size sections whose particles underwent large changes leading to unrealistic negative concentrations. Their appropriate mass is redistributed to size sections upstream of the filtered bins. While this introduces moderate numerical diffusion in terms of the prognostic mass mixing ratio in subranges of the size distribution, the method avoids numerical dispersion which is a common problem in many numerical formulations to solve competing aerosol growth processes (e.g. Tsang and Brock, 1983). The scheme is simple in its implementation; further details are given in Hommel (2008). In comparison to other state-of-the-art aerosol aerosol modules Kokkola et al. (2009) showed that this approach fairly well reproduces the growth of particularly ultra-fine particles under stratospheric background conditions and when the stratosphere is moderately contaminated by additional sulphur.

Brownian coagulation is considered following a semi-implicit mass conserving formulation by Timmreck and Graf (2000). Unlike in other models (e.g. Stier et al., 2005), intermodal coagulation is not restricted.

The modularised integration of SAM2 into its host model provides access to non-microphysical aerosol sources and sinks which were defined for ECHAM5's standard aerosol module HAM (Stier et al., 2005). Processes of sedimentation, dry and wet deposition are described in Stier et al. (2005) and were adapted to resolve the aerosol size by fixed sections instead of log-normal functions. Global surface emissions of natural and anthropogenic sulphur are taken from the AeroCom database and represent year 2000 conditions (Dentener et al., 2006). Like in ECHAM5-HAM 2.5% of the total emitted sulphur is treated as direct emission of primary particulate sulphate.

GMDD
3, 1359–1421, 2010

Emissions of primary sulphate from shipping and industry are partitioned between the accumulation and coarse modes of the aerosol size distribution. Other primary particulate sulphate emissions are attributed to the Aitken and accumulation mode. Volcanic emissions are considered from explosive and continuously degassing volcanoes (Halmer et al., 2002; Andres and Kasgnoc, 1998). Emissions from exceptional volcanic eruptions which inject large quantities of sulphur directly into the stratosphere are not considered in this study. The flux of dimethyl sulphide (DMS) from the marine biosphere is calculated as in Kloster et al. (2006) from prescribed monthly mean DMS sea water concentrations according to Kettle and Andreae (2000). Terrestrial biogenic DMS fluxes are prescribed based on monthly means (Pham et al., 1995).

The mixing ratio of carbonylsulphide (OCS) in the atmosphere is prescribed based on climatological monthly means taken from a transient run of ECHAM4-SAM, which was interactively coupled to the chemical transport model CHEM. In this simulation OCS emissions were held constant, yielding a surface mixing ratio of 520 pptv (SPARC/ASAP, 2006).

2.3 Chemistry module

The chemistry module employs the sulphur cycle of Feichter et al. (1996) in regions of the atmosphere below the tropopause and a scheme based on a sulphur chemistry extension of the chemical transport model CHEM (Steil et al., 2003; Dameris et al., 2005) in model levels attributed to the tropopause and above. The tropospheric sulphur cycle takes into account the aqueous phase transformation of SO_2 into sulphate in stratiform and convective clouds as well as homogeneous reactions of the day and night time oxidation of DMS and SO_2. Oxidants and, in the stratosphere, photolysis rates are prescribed based on zonal and monthly mean data sets. In the troposphere, concentrations of OH, H_2O_2, NO_2 and O_3 are taken from a climatology of the chemistry transport model (CTM) MOZART2 (Horowitz et al., 2003). In the stratosphere, OH, NO_2, and O_3 concentrations as well as photolysis rates of OCS, SO_2, SO_3, and O_3 originate form a climatology of the chemistry climate model MESSy (Jöckel et al.,

GMDD
3, 1359–1421, 2010

2005). The rate of H_2SO_4 photolysis in the UV range was estimated according Turco et al. (1979) and Rinsland et al. (1995) based on the MESSy calculated photolysis rate of HCl. Treating photolysis rates offline excludes the verification of recently proposed mechanisms of H_2SO_4 photolysis by visible light (Vaida et al., 2003; Mills et al., 2005a). Reactions and reaction rates are listed in Table 1.

2.4 Observational data

The model is evaluated with satellite-measured integral aerosol quantities, size resolved in situ aerosol measurements and precursor observations from several campaigns. Our analysis focusses on the validation of the aerosol size dependent integral quantities surface area density (SAD), volume density (VD), and effective radius (R_{eff}). The satellite data sets described below may contain other information as well, which are not considered here due to their higher retrieval uncertainties. We also do not take into account the SPARC ASAP/CCMVal stratospheric aerosol climatology (SPARC/ASAP, 2006, http://www.pa.op.dlr.de/CCMVal/Forcings/CCMVal_Forcings_WMO2010.html) because the product is only robust for aerosol surface densities.

In this paper, integrated aerosol quantities are compared to stratospheric aerosol climatologies provided by the University of Oxford (PARTS, 2004; Wurl et al., 2010), hereinafter referred to as UOX, and the NASA AMES Laboratory (Bauman et al., 2003a,b), hereinafter referred to as AMES. The data sets give information about the integrated parameters surface area density, volume density, effective radius, total concentration as well as the size distribution geometric radius and distribution width.

In both data sets aerosol size parameters are retrieved from extinction profiles measured with a sun occultation instrument during the Stratospheric Aerosol and Gas Experiments (SAGE) II, aboard the ERBS satellite (McCormick, 1987). The instrument operated from October 1984 to August 2005, providing the so far longest record of global stratospheric aerosol load. The latitudinal coverage of the measurements is approximately 70° S to 70° N. In the vertical, the data were processed in 0.5 km intervals.

GMDD
3, 1359–1421, 2010

The AMES climatology considers data from km above the tropopause only. In the UOX solution all extinction profiles were taken into account that passed a quality screening. Thus, the UOX climatology provides data within and potentially below the tropopause. Since the AMES climatology ends in August 1999, our analysis is build upon 1998 data which are seen as representative for the stratospheric background after the volcanic eruption of Mt. Pinatubo in 1991 (Deshler et al., 2006; SPARC/ASAP, 2006).

The AMES climatology combines the four wavelength extinction measurements from SAGEII with extinction profiles at 12.82 µm from the Cryogenic Limb Array Etalon Spectrometer (CLAES; Roche et al., 1993), which, in particular, has advantages in the detection of volcanic aerosol. The algorithm retrieves the effective radius, surface area, volume density, and the width of a unimodal log-normal size distribution by examining satellite-measured extinction ratios to pre-computed values utilising a look-up table in combination with a parameter search technique. As Bauman et al. (2003b) showed, in the volcanically quiescent stratosphere AMES retrieved aerosol surface area is a few percent larger than in the climatology of Thomason et al. (1997) which is based on Principal Component Analysis (PCA; Thomason et al., 1997; Steele et al., 1999).

In the UOX climatogy an inversion technique is applied based on the Bayesian Optimal Estimation (BOE) theory. Details on the method are given in Wurl et al. (2010). The BOE approach combines a priori knowledge of measured particle size distributions (Deshler et al., 2003a) with spectral aerosol extinction measurements. That makes the BOE solution sensitive to fine mode particles which are practically invisible for the spectral instrument (Kent et al., 1995; Steele et al., 1999). A further strength of the BOE method are error estimates as part of the retrieval process. In contrast, other inversion techniques like PCA attract solutions with a systematic bias (Steele et al., 1999). Wurl et al. (2010) showed that the BOE method is applicable in the presence of large experimental noise, what makes it favourable to retrieve the size of background aerosols. BOE retrieved surface areas and volume densities are 20 to 50% larger than PCA solutions of the operational SAGE II retrieval. They are less biased to data inferred from in situ observations. With respect to the discrepancy found in aerosol key quantities from

GMDD
3, 1359–1421, 2010

the different observation techniques (SPARC/ASAP, 2006), this is a clear advantage in improving the quality of globally monitored stratospheric background aerosols.

In situ measurements of aerosol quantities are inferred from optical particle counter (OPC) measurements in the stratosphere over Laramie (Wyoming, 41.3° N, 105.7° W). To date the Laramie record is the most coherent in situ observation (see SPARC/ASAP, 2006, and references therein). The counter, operative since 1971, measured stratospheric particle number concentrations at $R \geq 0.15$ and 0.25 µm. In 1989 the instrumentation was redesigned, now being able to resolve aerosol spectra in 12 channels from ≥0.15 to 2.0 µm. A condensation nuclei (CN) counter simultaneously measures particles with a radius of 10 nm ± 10%. Further details on the instrumentation and error estimates of derived aerosol quantities are given in Deshler et al. (2003a).

The modelled abundance of SO_2 and gaseous H_2SO_4 are compared with data from literature. In addition, the modelled abundances of SO_2 is compared to measurements taken during the Stratospheric Aerosol and Gas Experiment (SAGE) III Ozone Loss and Validation Experiment (SOLVE), conducted from December 1999 to March 2000 (e.g. Lee et al., 2003). SO_2 was measured by a chemical ionisation mass spectrometer (CIMS; Hunton, 2000) onboard the NASA research aircraft DC-8. The detection limit was approximately 25 pptv. The flights were made in the Arctic high latitudes and occasionally in the mid-latitudes at altitudes between 9 and 13 km. SOLVE data were obtained from NASA's ESPO archive (http://espoarchive.nasa.gov/archive). Of the ~11 000 samples for SO_2, approximately only one fifth were made below the tropopause and are not considered in our analysis. The data include samples from the volcanic plume of the Icelandic volcano Hekla, which erupted on 26 February 2000. In the morning of the 28th, the research aircraft passed the plume in a transit flight from Edwards AFB to Kiruna, Sweden, and also several days later volcanic signals are apparent (Rose et al., 2003).

GMDD
3, 1359–1421, 2010

2.5 Experiment setup

The model was integrated for 17 years, starting in January 1990. To shorten the model's spin-up period, prognostic aerosol components were initialised from a zonally averaged aerosol mass mixing ratio which was derived from the climatological mean volume density of the UOX SAGE II climatology. We assumed the aerosols throughout the stratosphere are homogeneously composed of 75% sulphuric acid with a density of 1.7 g cm^{-3}. The total mixing ratio was distributed to the size sections assuming an unimodal size distribution following Pinnick et al. (1976) with a mode radius of 0.0725 µm and a standard deviation of 1.86. Prognostic sulphate precursors were not initialised. Instead, the atmospheric abundance of DMS, SO_2 and H_2SO_4 is formed from boundary layer fluxes during the model integration.

Initialising aerosols rather than synthesise adequate abundances in the stratosphere solely from surface emission fluxes requires an assessment of the model's prognostic aerosol parameters in respect of their potential drift. We analysed the evolution of each size section's aerosol mixing ratio and other quantities from the free troposphere (~350 hPa) to altitudes (~3 hPa), where sulphuric acid aerosols are no longer thermodynamically stable due to elevated H_2SO_4 vapour pressures. Shown in detail in Hommel (2008), we found that all diagnosed parameters are balanced in the sixth year of integration. The following eleven years are the base for our model climatology.

3 Results and discussion

3.1 Global budgets

Figure 1 shows a schematic diagram of the global budget of prognostic sulphur constituents based on annual means of the last year of integration. Atmospheric lifetimes are given as global residence times. As noted before, DMS oxidation is constrained to the troposphere and OCS mixing ratios are prescribed. In the budget

GMDD
3, 1359–1421, 2010

diagnostics special consideration is given to ECHAM5's standard aerosol module HAM (Stier et al., 2005; Kloster et al., 2006) since both models use identical tropospheric process parametrisations and surface emission flux strengths. Hence, apparent differences in conversion rates diagnosed from both models are directly attributed to module specific treatments of aerosol dynamics.

With the explicit consideration of aerosol processes in the stratosphere, both the calculated global mean burden of sulphate aerosol and the lifetime are ~17% larger than in ECHAM5-HAM. Nevertheless the values are in the range of predictions from other global models, where aerosol processes are more or less constrained to the troposphere (Table 2). In the stratosphere Takigawa et al. (2002) diagnose an annual mean burden of sulphate aerosol of 0.149 Tg(S) from the CCSR/NIES aerosol coupled middle-atmosphere AGCM. This corresponds well with 0.148 Tg(S) derived in this study (17% of the total aerosol burden). However, the global annual mean burden of sulphate aerosol in Takigawa et al. (2002) with 0.36 Tg(S) is 60% smaller than in our model. Besides a different handling of source strengths, potentially the neglected tropospheric aqueous phase chemistry in the CCSR/NIES model accounts for this distinct discrepancy. It is widely approved that aqueous phase chemistry converts approximately two thirds of the emitted SO_2 to sulphate (Chin et al., 1996; SPARC/ASAP, 2006), see discussion below. Pitari et al. (2002) model a 2% higher stratospheric aerosol burden (0.151 Tg(S)) in a hybrid AGCM/CTM, resolving the size of sulphate aerosol by a sectional method with 15 bins. They refer to an estimated stratospheric aerosol burden of 0.156 Tg(S) based on SAGE I/SAM II data (Kent and McCormick, 1984) from 2 km above the tropopause for the year 1979, a year in which the stratosphere was near background after the volcanic eruption of Fuego in 1975. Comprehensively diagnosed are prognostic sulphur compounds and their transformation rates in the 2-D model AER (Weisenstein et al., 1997; SPARC/ASAP, 2006). AER also follows the sectional approach. In the standard set-up 40 bins resolve the aerosol size range from 3.9×10^{-4} µm to 3.2 µm. Dependent on parametrisations of tropospheric processes AER predicts a stratospheric aerosol burden ranging from 0.08 to 0.221 Tg(S),

GMDD
3, 1359–1421, 2010

with lower numbers calculated without additionally imposed fluxes of SO_2 and sulphate particles from the troposphere to the stratosphere.

Model predicted deposition rates of sulphur compounds differ not more than 10% from ECHAM5-HAM, except that the flux of sedimenting particles is a factor two weaker in our model. An overestimation of sedimentation rates from modal aerosol modules was also highlighted by Weisenstein et al. (2007) in a 2-D model intercomparison study under stratospheric conditions. The aqueous phase production of sulphate in tropospheric clouds is 6% larger than in ECHAM5-HAM and accounts for 65% of the total global sulphate production, which is in the ballpark of other studies (e.g. Pham et al., 1995; Penner et al., 2001; Liu et al., 2005). Relative to the transformation rates of 2-D model AER as shown in SPARC/ASAP (2006), in our simulation the stratospheric SO_2 oxidation is one order of magnitude larger. Differences in the in the three-body reaction oxidising SO_2 by the hydroxyl radical OH (see Weisenstein et al., 1997) may explain this relatively large discrepancy between both models.

In altitudes, where H_2SO_4 is supersaturated, the residence time of sulphuric acid vapour is considerably shorter than that of SO_2. In our simulation a three times longer lifetime of gaseous H_2SO_4 is predicted than diagnosed from ECHAM5-HAM (Stier et al., 2005; Kloster et al., 2006). This is clearly attributed to the extended vertical representation of the atmosphere in the AGCM MAECHAM5, because, as shown later in Sect. 3.2, above 30 km (which is the TOA in the in the studies performed with ECAHM5-HAM) the mixing ratio of gaseous H_2SO_4 is several orders of magnitude larger than below. In our simulation 98% of the global total sulphuric acid vapour condenses onto existing particles, only 0.1% nucleates and the remaining part deposits in the planetary boundary layer. Compared to ECHAM5-HAM, the mass transfer of H_2SO_4 from the gas to the particle phase via new particle formation is 3.6 times weaker in our model. This is due to differences in the sequential processing of competing aerosol microphysics processes. Investigating box model versions of the modules HAM and SAM2, Kokkola et al. (2009) showed that the sequential processing of HAM is more robust with respect to steep gradients in the oxidation rate of SO_2, e.g. as found in volcanic plumes. In the

GMDD
3, 1359–1421, 2010

stratospheric background, however, predicted aerosol size distributions from both modules are almost indistinguishable in the accumulation and coarse mode. Also the size of fine particles ($R < 0.01\,\mu m$) is better represented in SAM2 than in HAM compared to a benchmark model. A potential method to further improve the treatment of the two processes condensation and nucleation, which compete for the available sulphuric acid vapour, is given in Hommel and Graf (2010). In this study it was shown that reserving a certain fraction of the available sulphuric acid vapour for nucleation significantly improves the SAM2's ability to capture particle growth under elevated levels of SO_2 in the stratosphere.

Interestingly, the modelled rate of evaporating sulphates in the stratosphere is almost twice as strong as the oxidation rate of OCS, which is suggested to stabilise stratospheric aerosol abundances above 25 km (SPARC/ASAP, 2006). Depending on its set up, the 2-D model AER predicts OCS oxidation fluxes from $0.032\,Tg(S)\,yr^{-1}$ (SPARC/ASAP, 2006) to $0.049\,Tg(S)\,yr^{-1}$ (Weisenstein et al., 1997). For the 3-D CCRS/NIES model Takigawa et al. (2002) diagnose $0.036\,Tg(S)\,yr^{-1}$. Our modelled OCS oxidation rate is less than half than in the other models, what seems to be caused by the offline treatment and superimposing of OCS mixing ratios with photolysis rates taken from another model (see also Sect. 3.2).

Photolysis of sulphuric acid vapour above 35 km is a major nonvolcanic pathway for the SO_2 abundance in the upper stratosphere and mesosphere (discussed in Sect. 3.2). In our study, $7\times10^{-3}\,Tg(S)\,yr^{-1}$ of the gaseous H_2SO_4 in the stratosphere is photolysed to SO_2. This is 1% of the total SO_2 which is oxidised to sulphuric acid vapour above the tropopause.

3.2 Aerosol precursor gases

In this section we compare results of the modelled abundance of the prognostic sulphate aerosol precursors SO_2 and sulphuric acid vapour against several observations and comparable model studies. We will concentrate on SO_2 and gaseous H_2SO_4. DMS concentrations in the LS are several orders of magnitude lower than in the troposphere,

GMDD
3, 1359–1421, 2010

and hence approximately negligible (Weisenstein et al., 1997). Prescribed fields are used for OCS.

During several field campaigns sulphur-bearing gases were measured in the troposphere, but were measured only sporadically in the stratosphere (reviewed in SPARC/ASAP, 2006). Early in situ observations of SO_2 (Meixner, 1984; Möhler and Arnold, 1992) and sulphuric acid vapour (Arnold and Fabian, 1980; Viggiano and Arnold, 1981; Arnold et al., 1981; Heitmann and Arnold, 1983; Arnold and Qiu, 1984; Schlager and Arnold, 1987; Möhler and Arnold, 1992; Reiner and Arnold, 1997) were conducted in the middle and upper stratosphere of NH mid-latitudes, some of them during volcanically active periods, e.g. the eruption of El Chichón in 1982. Rinsland et al. (1995) reported SO_2 profiles in the middle stratosphere provided by the ATMOS infrared spectrometer onboard the NASA Space Shuttle for SPACELAB 3 in 1985. After the massive eruption of the Philippine volcano Mt. Pinatubo in June 1991, a series of flight campaigns measured the abundance of several gases, including SO_2 (SPARC/ASAP, 2006). In contrast to the above mentioned early in situ measurements, both spatial coverage and temporal resolution of nowadays airborne sampling techniques increased, but their altitudinal coverage is still often limited to the free troposphere. With respect to newer airborne observations, we choose to validate the modelled abundance of SO_2 with previously unpublished measurements made during the NASA SAGE III Ozone Loss and Validation Experiment (SOLVE), conducted at Arctic high latitudes from December 1999 to March 2000. The majority of the data collected in 14 missions were sampled above the tropopause up to 13 km altitude.

In Fig. 2 a composite of calculated vertical profiles at the equator, the NH mid and high latitudes of all sulphur constituents is shown. In Fig. 3 we compare our model results to other models and specific in situ observations of stratospheric SO_2 and sulphuric acid vapour, and in Fig. 4 we evaluate LS SO_2 mixing ratios with data collected during SOLVE. Compared to available measurements and appropriate model data, MAECHAM5-SAM2 reproduces distinct features in the atmospheric distribution of SO_2 and gaseous H_2SO_4. In the lower stratosphere the rapid and effective photochemical

GMDD
3, 1359–1421, 2010

transformation of SO_2 to H_2SO_4 and the subsequent partitioning of the latter into aerosol droplets results in the formation of distinct minima in the vertical profiles of both gases, whereas the aerosol mixing ratio increases (Fig. 2). In central and upper regions of the aerosol layer, between 20 and 35 km, photodissociation of OCS increases the stratospheric SO_2 abundance. In this region of the stratosphere, the positive gradient of H_2SO_4 gas mixing ratios is more pronounced than those of SO_2. Due to the positive gradient in the stratospheric temperature above the cold point tropopause, both the oxidation rate of SO_2 and the H_2SO_4 vapour pressure increase with altitude. The latter leads to a with altitude strongly decreasing mass transfer to the particle phase, and more H_2SO_4 is held in the gas phase. When H_2SO_4 is subsaturated aerosols evaporate completely, resulting in a strong negative gradient in the aerosol mixing ratios above 30 km (Fig. 2). Between 37 and 40 km, H_2SO_4 released into the gas phase reaches peak mixing ratios of ~70 pptv. Slightly lower values are found in mid and high latitudes. Above 40 km, sulphuric acid vapour is photolysed to SO_3, which in turn rapidly photolyses to SO_2 (Burkholder and McKeen, 1997), ultimately forming a reservoir of SO_2 in the stratosphere above 40 km.

Measurements by the ATMOS infrared spectrograph onboard the NASA Space Shuttle for SPACELAB 3, made from April to May 1985 between 26 and 32 N, confirm the formation of such a SO_2 reservoir (Fig. 3). However, the data also revealed a negative gradient in the SO_2 mixing ratio around the stratopause (Rinsland et al., 1995). This gradient cannot be reproduced in our experiment. Instead, the SO_2 mixing ratio remains approximately constant in heights above 50 km. Whether this is due to an unresolved mechanism in the modelled photochemistry or due to a missing sink in the microphysics, e.g. vapour uptake by meteor debris (e.g. Mills et al., 2005b; Turco et al., 1981), remains speculative since neither of the processes postulated in the literature is confirmed experimentally.

Also in the LS modelled SO_2 mixing ratios are in good agreement with observations made during SOLVE between December 1999 and March 2000 (Fig. 4). SOLVE data are affected by the eruption of the Icelandic volcano Hekla on 26 February 2000 (Rose

GMDD
3, 1359–1421, 2010

et al., 2003). However, in our analysis volcanic samples where not excluded from the data, since our statistical analysis revealed that the signal of the UT/LS background concentration of SO_2 is robust in the data set and showing a well pronounced normal distribution at all altitudes: The median of the measured background concentration in the LS with 35 pptv (0.25 and 0.75 percentiles at 28.3 and 43.3 pptv) is 20% below the analysis of Lee et al. (2003), which excluded data above 200 pptv and considered also samples made in the UT. In Fig. 4, outliers (represented by larger spread of the data as well as mean values lying beyond the interquartile range, IQR, of the data) are clearly marking measurements affected by volcanic SO_2. Modelled SO_2 is more biased relative to SOLVE in the lower latitudes. At 46° N, between 10 and 11 km, MAECHAM5-SAM2 overpredicts the mixing ratio by 58% in DJF and by 150% in MAM. In higher latitudes most of the model data are at least within the IQR of the observations.

A detailed investigation how sulphate aerosol models predict stratospheric SO_2 mixing ratios in the tropics and subtropics was given in SPARC/ASAP (2006). With minor exceptions due to the different treatment of chemical and physical processes in the models, the predicted profiles are in qualitative agreement. The spread of the data, however, is rather large between the models. Some of the models are also distinctly biased relative to the ATMOS observations (Rinsland et al., 1995) in the middle and upper stratosphere. As seen in the Figs. 2 and 3 our model does not predict a distinct maximum in the (sub)tropical SO_2 mixing ratio around the 28 km altitude, which was more pronounced in the model results shown in SPARC/ASAP (2006) and Mills et al. (2005a).

For SO_2 the Mills et al. (2005a) model clearly underpredicts the ATMOS observations (Fig. 3a) whereas sulphuric acid vapour is within the range of observations above 28 km (Fig. 3b). Below, where aerosol concentrations are largest, Mills et al. (2005a) clearly overpredicts gaseous H_2SO_4 by more than 50%. MAECHAM5-SAM2 is in agreement with the observations (Fig. 3b), however the spread of the measurements, which exist for the near-background pre-Pinatubo period only, is larger than one order of magnitude above 28 km.

GMDD
3, 1359–1421, 2010

Vertical profiles of SO_2 in the tropics as predicted by the 2-D model AER (Weisenstein et al., 1997) exhibit vertical displacements in the altitudes showing maxima and minima compared to our simulation. The displacements prevail in the extratropics and are in the order of −6 km, relative to our data, from above the tropopause to heights of ∼35 km. The profiles for sulphuric acid vapour are in qualitative agreement, in the tropics AER shows ∼50% larger values than our model but in the NH mid-latitudes the bias is marginal up to 32 km height. The vertical profiles of SO_2 are in good agreement to the 3-D Japanese CCRN/NIES model in the tropics and NH mid-latitudes (Takigawa et al., 2002). In our simulation, higher mixing ratios are found in the tropical tropopause layer (TTL), and up to 80% lower SO_2 mixing ratios occur where the stratospheric aerosol abundance is largest (above 20 km). Due to missing links in the chemistry, the Takigawa et al. (2002) model does not reproduce the stratospheric reservoir of SO_2 above 30 km. Their H_2SO_4 in the gas phase is much lower than in our simulation. The 1-D stratospheric aerosol model of Turco et al. (1979) and Toon et al. (1979) predicted profiles for SO_2 and sulphuric acid vapour very similar to those shown in Fig. 2. Differences are seen in the representation of upper stratospheric mixing ratios of SO_2, which are up to one order of magnitude larger in our simulation, and of gaseous H_2SO_4, which do not show a distinct negative gradient above 26 km.

A model-intercomparison in SPARC/ASAP (2006) revealed only minor differences between the models regarding the OCS abundance in the atmosphere. Models agree to a large extend with observations made in the stratosphere. Our offline data are based on these published data, and so it is assumed that OCS mixing ratios are well represented in our model.

Despite different representations of stratospheric dynamics in the models mentioned above, 1-D models behave like global models with respect to the representation of the stratospheric precursor abundance. Significant differences, which exist in the modelling of some of the key characteristics seem to result from parametrised processes and missing links in sulphur chemistry schemes.

GMDD
3, 1359–1421, 2010

3.3 Global aerosol distribution

The annual mean burden of modelled sulphate aerosol is shown in Fig. 5. Tropospheric sulphate dominates, since, as analysed in Sect. 3.1, stratospheric aerosol contribute to less than 20% to the global annual mean sulphate mass of the atmosphere. The modelled sulphate burden is in agreement with sulphate components of other model studies which utilise comparable emission scenarios (e.g. Stier et al., 2005; Ma and von Salzen, 2006). Particulate sulphate is concentrated in regions of high anthropogenic sulphur emissions, i.e. industrialised regions in South East Asia, Europe, and Northern America. Significant dispersion of aerosols to Northern Africa and the Middle East occurs in the planetary boundary layer, which is is also seen in aerosol mixing ratios at the surface (Fig. 6a). Zonal homogenisation of the atmosphere's aerosol abundance increases with altitude (Fig. 6b and c). In the stratosphere (Fig. 6c), the aerosol layer is well stratified and, due to low air density, the mixing ratio in the tropics is approximately as high as in the terrestrial boundary layer. In the free troposphere the mixing ratio of sulphate aerosol is approximately one order of magnitude lower.

The annual mean total particle number concentration (N_T) is dominated by ultra-fine particles throughout the atmosphere. As in other model studies, e.g. Ma and von Salzen (2006), at the surface the global distribution of the aerosol number concentration is very well correlated with the aerosol mixing ratio. Largest number concentrations are found over continental regions and are associated with anthropogenic pollution. Primary emissions occur mainly in the accumulation mode, thus are less reflected in the total number concentration near the surface (with exceptions in continental regions near the equator) and in the total sulphate aerosol mixing ratio. The global dispersion of N_T in the boundary layer is less pronounced than in the mixing ratios, indicating a rather fast ageing of aerosols, which is associated with a reduction of ultra-fine particle number concentrations. In East Antarctica and over Greenland, where the aerosol mixing ratio is lowest in the model, number densities of more than 5×10^3 cm^{-3} are found. Here aerosols are formed due to binary homogeneous nucleation in low temperature/high

GMDD
3, 1359–1421, 2010

relative humidity environments (see Easter et al., 2004; Spracklen et al., 2005; Ma and von Salzen, 2006).

N_T increase with altitude, reaching maxima in the mid-latitude free troposphere, where binary homogeneous nucleation rates are largest (Stier et al., 2005; Spracklen et al., 2005; Makkonen et al., 2009). Given the importance of new particle formation for the total particle concentration in the atmosphere, above the boundary layer a pronounced anti-correlation between the total number density and the mixing ratio of sulphate is seen in Fig. 6. This becomes apparent in the stratosphere, where the rates of new particle formation are largest in the spring time polar vortices (see Fig. 7b and c).

Figure 7 shows zonal means of the seasonal averaged aerosol mass mixing ratio, nucleation rate, and nucleation mode number density for the 11 year analysis period. The tropical stratospheric reservoir (TSR; Trepte and Hitchman, 1992; Hitchman et al., 1994), a region which is quasi isolated from meridional transport, as well as the isolated air masses in the SH polar vortex are clearly seen in the modelled aerosol mixing ratio (Fig. 7a). Distinct staircase patterns found in the subtropical mixing ratio result from interactions between advective transport by the mean meridional circulation, the meridional circulation associated with the quasi-biennial oscillation, the semi-annual oscillation, and effects of isentropic mixing by the absorption of planetary wave energy (Baldwin et al., 2001). In agreement with findings of Hitchman et al. (1994) on the basis of aerosol data from the space-borne SAM and SAGE instruments, a transport regime has been identified in the lower stratosphere, where particles are transported poleward and downward during winter. These patterns persist into subsequent equinoctial seasons and are most pronounced in the NH. The same authors deduced an upper transport regime in the tropics during summer (above 22 km), which is also reflected in our results in poleward oriented mixing ratio gradients in the upper branches of the TSR.

GMDD
3, 1359–1421, 2010

There is no evidence from the modelled aerosol mixing ratio isolines that the high abundance of aerosols within the TSR is supplied by sulphate particles of tropospheric origin, transported into the LS by tropical upwelling. Instead, in boreal summer a significant flux of tropospheric particles reaches the LS in the subtropics and midlatitudes. The regions, where in our model aerosols are uplifted into the LS correspond to cells of tropospheric convection over the Asian Monsoon/Tibetan Plateau region, which is one of the main pathways for the cross-tropopause transport of atmospheric moisture and other trace gases (see Fueglistaler et al., 2009, and references therein). Aerosols reaching the LS are transported poleward within the lower stratospheric transport regime, but a significant amount of particles also reaches the tropics via the upper Monsoon's anticyclone (Bannister et al., 2004; Fu et al., 2006).

Preferred regions where new sulphate droplets are formed in the model are the free troposphere above 500 hPa as well as the winter and spring time polar vortices above the 70 hPa pressure altitude (Fig. 7b). Within a few kilometres above the tropopause, where temperatures are as low as 200 K, the Vehkamäki parametrisation of binary homogeneous nucleation predicts a minimum in the nucleation rate, which is not seen in studies using the models ECHAM4-SAM (Timmreck, 2001) or AER (Weisenstein et al., 1997). A second maximum in tropical stratospheric nucleation rates is seen between 60 and 50 hPa, leading to remarkably high nucleation mode number densities of $<10\,\mathrm{cm}^{-3}$ throughout the tropical lower stratosphere, up to the 30 hPa pressure altitude. Brock et al. (1995) showed particle mixing ratio profiles from measurements in the tropics in March 1994, when Mt. Pinatubo aerosols declined to near-background levels (the data were attributed as cleared from volcanic aerosol). The profiles exhibit that total number mixing ratios of volatile particles are largest in the free troposphere, but also reveal a minimum directly above the tropopause and a second maximum above, centred around 70 hPa. The nucleation rate estimates by Brock et al. (1995), however, cannot resolve the vertical resolution of our simulation, hence do not show the minimum above the tropopause as seen in Fig. 7b. Given these observations and our results, it is likely that due to tropical upwelling ultra-fine particles with tropospheric

GMDD
3, 1359–1421, 2010

origin contribute to the formation and maintenance of a stable stratospheric aerosol layer also in volcanically quiescent periods. But our calculations also reveal that a significant portion of TSR aerosol might be formed in the tropical LS before it ages in higher altitudes and becomes mixed to the extratropics.

High CN concentrations in the spring time polar vortices are observed in altitudes well above the aerosol layer (reviewed in SPARC/ASAP, 2006). Zhao and Turco (1995) first suggested, using a 1-D model, that the formation of an Antarctic stratospheric CN layer strongly depends on the subsidence of a non-condensable gas like SO_2 in the polar night vortex. Mills et al. (1999) and Mills et al. (2005a) showed that in the upper stratosphere SO_2 originates from photolysis of H_2SO_4 and is transported poleward with the mean meridional circulation. In descending air masses of the Antarctic polar vortex SO_2 is rapidly oxidised when sunlight returns in spring, hence it triggers the formation of the polar stratospheric CN layer. Furthermore they showed that, nearly independent on the photochemistry mechanisms, which are thought to account for a stabilised stratospheric reservoir of SO_2, new particle formation is likely also in polar winters according to the classical nucleation theory. However, in the southern polar vortex a sharp increase in the CN concentration is not predicted until enough gaseous H_2SO_4 is supplied for condensation in late August.

In our model this formation of polar stratospheric CN layers is reproduced (Fig. 7b). In the Arctic polar vortex nucleation occurs in altitudes between 1 and 10 hPa also in winter, with stronger rates at the end of the season. In March, nucleation rates are of similar strength (not clearly reflected in Fig. 7b due to seasonal averaging), but centred at lower altitudes around 20 hPa. In the Antarctic stratosphere significant nucleation rates are seen at 10 hPa in April and July. When sunlight returns in late August, rates of new particle formation increase to $5\times10^{-3}\,cm^{-3}\,s^{-1}$ in descending air masses below 10 hPa and persist until late October. Over both poles polar stratospheric CN layers are formed readily after nucleation events produce high concentrations of particle nuclei (10 to several 100 particles per cm^{-3}) because coagulation efficiently removes ultra-fine particles, so that aerosols are rapidly growing to detectable sizes, see Sect. 3.5.

GMDD
3, 1359–1421, 2010

In Antarctica MAECHAM5-SAM2 predicts peak CN concentrations slightly higher than observed. However, location, subsidence as well as depletion of the CN layer correspond well with CN counter observations by e.g. Hofmann et al. (1989).

Meridional transport of stratospheric aerosols is not restricted to the motion of air masses relative to the mean meridional circulation of the stratosphere. From Fig. 7c, an efficient lateral mixing of ultra-fine particles from the polar vortices into stratospheric mid and low latitudes due to Rossby wave activity (e.g. Waugh et al., 1994) can be deduced. There is evidence for a stronger wave activity in the NH since in the middle stratosphere gradients in number density appear stronger than in the SH. Although no nucleation occurs in those regions of the stratosphere, ultra-fine particles mixed to mid-latitudes are growing to larger sizes or even evaporate, dependent on the partial and vapour pressure of H_2SO_4 (Fig. 8).

The upper branch of the stratospheric aerosol layer is not only a region where aerosols shrink in size due to the release of sulphuric acid and water into the gas phase (Fig. 8). Here the model predicted climatologies of the zonal mean H_2SO_4 vapour pressure as well as the concentration of sulphuric acid vapour, which is transferred from the gas to the particle phase (condensation) and vice versa (evaporation), are shown. The ability of sulphuric acid vapour to condense onto preexisting particles is strongly reduced at the cold tropopause. In the lower stratosphere, from a few kilometres above the tropopause to regions where sulphate aerosol evaporates, the mass transfer onto the particles remains remarkably constant. This region corresponds to the central region of the aerosol layer. The non-existence of meridional gradients in the mass transfer concentration of H_2SO_4 condensation implies that, at least in the stratospheric background, condensational growth is approximately constant over broad regions of the aerosol layer. Consequently, one may assume that the shape of particle size distributions in those region of the LS is similar from the tropics to the extratropics. Thus we investigated aerosol size distributions for all latitudes in the LS where the condensational flux is between $1\times10^3\,cm^{-3}$ and $5\times10^3\,cm^{-3}$. We found that for approximately constant nucleation rates the balance between the microphysics processes growth due

GMDD
3, 1359–1421, 2010

to H_2SO_4 condensation and growth due to coagulation does not change significantly at all latitudes in this region (except in high latitudes near 30 hPa, where small particles evaporate quickly). When the nucleation rate increases, coagulation becomes a more effective sink for aerosols with $R < 0.07$ µm.

In the mid latitudes, at altitudes where sulphate droplet evaporation is largest (Fig. 8c) also an enhanced H_2SO_4 vapour condensation is found (Fig. 8b). Breaking waves in the "Surf Zone" (McIntyre and Palmer, 1984) yield fluctuations in the stratospheric temperature, which in turn changes the direction of H_2SO_4 mass transfer onto or off the particle phase. Such fluctuations last a couple of days. In the averaged climatologies of Fig. 8b and c, regions of vapour condensation above 20 hPa overlap with regions where aerosols evaporate. Thereby H_2SO_4 condensation stabilises stratospheric aerosols until the particles are further transported poleward, where vapour pressures are higher and where they ultimately evaporate.

Detailed investigations of the interannual variability of the modelled stratospheric aerosol layer, in particular on interactions with the quasi-biennial oscillation, are given in a companion paper (Hommel et al., 2010).

3.4 Stratospheric aerosol climatology

In this section, the model climatology of integrated aerosol quantities is compared with data retrieved from the spaceborne SAGE II instrument. The integral of the model results is taken for particles exceeding 50 nm in radius in order to achieve comparability with detection limitations of optical instruments (Dubovik et al., 2000; Pitari et al., 2002; Thomason et al., 2008; Kokkola et al., 2009).

From Fig. 9 it can be seen that relative to SAGE II higher moments of the aerosol distribution are better represented in the model than lower moments. The variability of the satellite retrieved second and third moments of the aerosol distribution (SAD and VD) is much larger than in the model, mainly due to its relatively coarse spatial resolution. This also affects the model's ability to reproduce strong meridional gradients, which are seen in particular in extratropical SAD's of the AMES retrieval. In the model

GMDD
3, 1359–1421, 2010

a distinct asymmetry in the meridional distribution of VD and SAD is found, whereas the effective radius does not differ much over the aerosol layer. Instead the SAGE II retrieved R_{eff} is larger on the northern hemisphere, lower values are seen south of the equator in both retrievals within a few kilometres above the tropopause. Here the model underestimates R_{eff} by more than 150%. Also the satellite derived R_{eff} exhibit a strong vertical gradient, with largest values found above the tropopause and low values in regions where sulphate droplets evaporate (above 27 km).

The asymmetry in the modelled second and third moment is explained as follows: As shown before, the modelled stratospheric aerosol layer is strongly influenced by convective uplift over the Asian Monsoon regions, which transports significant amounts of particles, formed and grown to Aitken mode sizes in the free troposphere, into the LS. Those particles increase the surface area and, to a lesser extend, the volume density. Due to the large numbers of those particles entering the LS, those particles also contribute to the total aerosol mass (Fig. 7a) due to further absorbing H_2SO_4 and growing to larger sizes. In the annual mean of the effective radius, however, this contribution is not reflected. This, and the homogeneity of the modelled R_{eff} have two reasons: first, due to the one-moment approach of the aerosol scheme (aerosol number is not prognostic, hence not conserved, Adams and Seinfeld, 2002), and, second, due to the operator splitting technique used to solve competing processes within relatively large global model time steps, the aerosol volume to surface relationship, which determines R_{eff} (e.g. Grainger et al., 1995), is relatively tied and not a function of altitude. Hence, the modelled effective radius is a constant when an aerosol population in a certain region of the stratosphere is not affected by external sources or sinks, i.e. new particle formation or vertical updraft of sub-population particles. We found a reduction of a few percent in the modelled R_{eff} during the summer months in the extratropical updraft regions of the LS. Their contribution to the zonal annual mean, however, is too weak to be noticeable.

In Fig. 10 the climatological zonal mean aerosol mass density (MD) as predicted by the model is compared with respective MD's derived from the two different SAGE II

GMDD
3, 1359–1421, 2010

climatologies. MD's of the latter were derived from volume densities as shown in Fig. 9, assuming that stratospheric sulphate aerosols are homogeneously composed throughout the stratosphere with a sulphuric acid weight percentage of 75% and a solution density of 1.7 g cm^{-3}. The model MD was diagnosed online, depending on the appropriate particle composition as predicted by the model's thermodynamical parametrisations.

The characteristic distribution of the aerosol MD in the LS is similar to those of the VD (Fig. 9 upper row) although meridional and vertical gradients appear stronger in the MD. The quantitative agreement between model and SAGE II is satisfying for this parameter, in particular in the NH. In the SH, poleward from midlatitudes below 18 km, a general underestimation of modelled MD's in the order of ~30% is seen.

Mass densities shown for the 2-D model AER in Weisenstein et al. (1997) are in qualitative and quantitative agreement to our study. MD's of the same model shown in SPARC/ASAP (2006) are ~35% larger in the extratropical lower stratosphere, also showing enlarged aerosol masses in the TTL. The latter feature is neither found in our data nor in SAGE II retrieved aerosol mass densities. Table 3 summarises values of this quantity from literature for northern hemispheric extratropics, including older work made on SAGE II measurements as well as estimates from in situ observations. Also here the overall agreement between models of different complexity and between models and observations is obvious. The aerosol mass is a very robust parameter, with less deviations between the models. Also the resolution of the discretised aerosol size spectrum seems to have a minor effect on the predicted MD. This can be derived also from Yue et al. (1994) for the pre-Pinatubo period, which as Kent et al. (1995) utilises an early version of the SAGE II retrieval algorithm. Results of Kent et al. (1995), however, are up to twice as large as other SAGE II and model data shown in Table 3. In situ measurements below 21 km are distinctly smaller. Kent et al. (1995) derive MD's from extinctions by applying a factor for the particle volume-to-extinction ratio. Yue et al. (1994) followed an approach very similar to our online diagnostics of MD: the extinction derived volume density was multiplied with thermodynamically calculated aerosol densities and normalised sulphuric acid mass fractions. To analyse whether the Kent

GMDD
3, 1359–1421, 2010

et al. (1995) assumption yields positive biased MD's is beyond the scope of this paper, but it is likely that this approach is very sensitive in a background stratosphere.

3.5 Comparison with in situ measurements

In this section we evaluate the vertical distribution of the modelled stratospheric aerosol abundance by comparing the model predicted aerosol size with in situ measurements from the ballon-borne optical particle counter (OPC) operated by the University of Wyoming (e.g. Deshler et al., 2003a). All data shown in this section are attributed to the location were the instrument is launched (Laramie, WY, 41.3° N, 105.7° W). Figure 11 compares model predicted annual zonal mean size distributions with OPC measured number concentrations of the individual OPC channels for 2006. For the calculation of the median from observed number concentrations we sampled the measurement data according to the layer heights as used in model postprocessing. Vertical whiskers denote the spread of the measurements from all soundings in the respective period. Fig. 11 exposes significant differences in the representation of Aitken mode particles at 70 and 50 hPa whereas the concentration of accumulation and coarse mode particles agree quite well with the observations. In this region of the aerosol layer, where aerosol mixing ratios are largest, the measured concentration of CN is approximately one order of magnitude larger than in the model. Above peak aerosol mixing ratios, at 30 hPa, model and observations are in good agreement over the whole size range. Here temperatures clearly exceed 210 K and nucleation rates are significantly smaller than below, although sufficient concentrations of sulphuric acid vapour would be available to form new particles (see Fig. 3). Towards the tropopause, the model slightly underestimates the number of accumulation mode particles while overestimating the number density of very large coarse mode particles. Below the tropopause, at 250 hPa, this negative bias becomes even more distinct. Consistent with findings of Makkonen et al. (2009), in the UT the Vehkamäki parametrisation of binary homogeneous nucleation predicts very high numbers of nucleation mode particles, tending to an overestimation in the modelled CN concentration in the free troposphere.

GMDD
3, 1359–1421, 2010

In central regions of the aerosol layer, bimodal aerosol size distributions are predicted. Towards the tropopause and below the shape of the size distributions transforms into monotonically decreasing curves since gas-to-particle partitioning overwhelms particle growth by coagulation.

An example of the seasonality in the size distributions is shown in Fig. 12 for the 50 hPa pressure altitude. Here the model data are climatological means of the grid cells above the geographical position of Laramie. Measurements are shown as medians of all soundings conducted from 1998 to 2006, re-binned according to the vertical resolution of the model. Again, the spread of the measured number densities is shown as whiskers. Moderate annual cycles in the number concentrations can be seen for particles with $R \leq 20$ nm. In the model the annual cycle is pronounced for ultra-fine particles with enhanced concentrations of freshly formed particles during summer. The growth of nuclei to detectable sizes is affected by coagulation rather than by condensation. Particle growth by coagulation is characterised by an effective reduction of the number of ultra fine particles, which is accompanied by a moderately decreasing standard deviation of an unimodal size distribution. Condensational growth, however, does not reduce the number of growing particles. It instead leads to an effective reduction of the spread of a size distribution (Jacobson, 1997). Hence, the formation of a distinct minimum in the model predicted size distribution within the nucleation mode is caused by an overestimated coagulation efficiency of small mode particles. In the observations an annual cycle is seen in the variability of the measured number concentrations, in particular for CN and particles with $0.2 \leq R \leq 0.8$ µm. The median of the data, however, does not vary significantly. The underprediction of CN concentrations is also known from other bin-resolved aerosol models, e.g. GLOMAP (D. Spracklen, personal communication, 2009), and neither is a feature related to stratospheric conditions nor to the model's underlying nucleation mechanism. The source of the problem is not yet clear. Further investigations on the modelling of the growth of ultra-fine particles under well defined conditions are necessary.

Figure 13 shows vertical profiles of the effective radius in the stratosphere

GMDD
3, 1359–1421, 2010

over Laramie. Data representing observations were retrieved from surface area and volume densities, which in turn were derived from size distribution fits to the measurements (ftp://cat.uwyo.edu/pub/permanent/balloon/Aerosol_InSitu_Meas/US_Laramie_41N_105W). Taking the relatively large uncertainties of the surface area and volume estimates of the measurements into account (Deshler et al., 2003a), the model reproduces the effective radius in the stratosphere reasonably well. In the model as well as in the observations the maximum effective radius is found where aerosol mixing ratios are largest (16 and 27 km). In the model this feature is reproduced only when the parameter is retrieved for the whole aerosol spectrum. However then R_{eff} is underestimated by at least a third. A better representation is achieved, in particular a few kilometres above the tropopause and above 25 km, when the spectrum is integrated for the visible range of optical instruments.

From the size distributions shown in the Figs. 11 and 12 and the relationships between the different diagnosed aerosol parameters in the preceding sections, it is obvious that "typical" stratospheric background aerosol size distributions are bimodal rather than unimodal, as often cited in literature (e.g. Pinnick et al., 1976; SPARC/ASAP, 2006). The first, very narrow mode is centred in the size regime where new particles are formed, i.e. $R < 0.01\,\mu\mathrm{m}$. The median radius of the second, much broader mode, is located in the accumulation mode regime below 0.1 µm. Fine mode particles do not only substantially contribute to integrated aerosol quantities with importance for heterogeneous processes in the stratosphere. They also affect the size of the area weighted effective radius, a measure widely used to interpret radiative properties of aerosols, because condensational growth of ultra-fine particles enlarges the number concentration in the Aitken mode and lower accumulation mode. Hence, they enlarge the aerosol surface area and, to a lesser extent, the volume density. The more particles are formed the smaller is the calculated effective radius. In addition to the insensitivity of SAGE II retrieved integrated aerosol size parameters to fine mode particles yielding negatively biased surface areas (Thomason et al., 2008), this relation also accounts for the discrepancy of integrated aerosol size quantities from model and SAGE II (Fig. 9),

GMDD
3, 1359–1421, 2010

which is largest for the effective radius. This relation also accounts for the underprediction of R_{eff} relative to the Laramie OPC measurements, since the latter were inferred from bimodal size distribution fits to the measured number concentrations for $R > 0.01\,\mu\mathrm{m}$.

4 Conclusions

The size resolved aerosol module SAM2, incorporated into the middle-atmosphere climate model MAECHAM5, has been applied to investigate the stratospheric aerosol layer during an eleven year volcanically quiescent period. The model is evaluated against in situ observations and SAGE II retrieved integrated aerosol size quantities for the period when Mt. Pinatubo aerosols settled to background levels after 1995.

In situ measured size distributions of stratospheric aerosols in the NH mid-latitudes are fairly well reproduced by the model. In regions of the aerosol layer, where aerosol mixing ratios are largest, model predicted CN concentrations are underpredicted, indicating an overestimated coagulation efficiency in the model. Because nucleation from the gas phase is a major source of new particles in the stratosphere during volcanically quiescent periods, model predicted size distributions of stratospheric aerosols show a distinct bimodal structure over large areas of the LS.

The agreement between model and SAGE II retrieved integrated aerosol quantities related to the size of particles improves for higher moments of the aerosol size distribution. Lower moments as the effective radius are significantly underestimated by the model in large areas of the stratosphere due to limitations of remote sensing instruments at the bottom end of the aerosol spectrum and a priori constraints in the retrieval methods which do not take the formation and growth of new particles into account. This confirms "key finding two" of the SPARC Assessment of Stratospheric Aerosol Properties (2006), that the obvious consistency between in-situ and satellite measurements in a volcanically perturbed stratosphere is not maintained in periods of very low aerosol load, when aerosol key quantities significantly differ between the systems.

GMDD
3, 1359–1421, 2010

Major characteristics of the dynamics of stratospheric aerosols are reproduced. Transport regimes of tropical stratospheric aerosol have been identified from modelled mixing ratio gradients and correspond to observational findings based on satellite extinction measurements. A major pathway where aerosols in the model reach the stratosphere, is convection driven transport in the Asian Monsoon region during boreal summer. While this mechanism is vital for maintaining stratospheric trace gas abundances including water vapour, from global monitoring of UT/LS aerosol quantities this extratropical cross-tropopause transport was not evident so far. New particles are formed mainly in the free troposphere. However, nucleation is not unlikely above the cold point tropopause, forming at least one order of magnitude fewer particles than in the UT. In polar spring, new particles are formed within the polar vortex in altitudes far above the tropopause, leading to well reproduced layers of sub-micron particles (CN layer) in the model. Consistent with observations, in subsequent equinoctial seasons those CN layers settle to lower altitudes and, when the aerosols are grown to larger sizes, are removed quickly from the stratosphere in diabatically descending air within the polar vortices or even re-evaporate. The incorporation of aerosols into and their removal via PSC's are not considered in the model. We also found significant concentrations of fine mode particles in the stratospheric "Surf Zone", where new particle formation is very unlikely. Those aerosols are transported from polar regions into mid- and low latitudes through meridional mixing induced by the dissipation of planetary waves on the edges of the polar vortices. This process is strongest on the winter hemisphere. In the evaporation regime of the stratospheric aerosol layer we found regions where the time mean sulphuric acid droplet evaporation comes along with H_2SO_4 vapour condensation due to small scale fluctuations in the stratospheric dynamics. This prolongs the aerosol lifetime in the "Surf Zone" so that particles are transported further poleward with the mean meridional circulation.

Despite the poor data base of observed sulphate precursor abundances in the UT/LS, the modelled concentrations of SO_2 and sulphuric acid vapour are in good agreement to measurements and are less biased than those of other models.

GMDD
3, 1359–1421, 2010

We report UT/LS measurements of SO_2 mixing ratios made in the NH mid and high latitudes on a NASA DC8 research aircraft during SOLVE in Winter 1999/2000. They give evidence that, at least in corresponding regions, the SO_2 abundance in the LS is captured well by the model.

From the results presented here we conclude that MAECHAM5-SAM2 is a suitable model for studies of the dynamics of stratospheric background aerosol. Its capability of treating other aerosol compounds than sulphate as well as its performance in scenarios of enhanced stratospheric sulphur loads of whatever reason remains subject of future model development and investigations.

Acknowledgements. This work was supported by the EC projects PARTS and SCOUT-O3. We thank Peter Braesike, Christoph Brühl, Terry Deshler, Marco Giorgetta, Hartmut Grassl, Don Grainger, Stefan Kinne, Silvia Kloster, Harri Kokkola, Shanhu Lee, Ulrike Niemeier, Declan O'Donnel, Benedikt Steil, Philip Stier, Manu Thomas, Larry Thomason, Hanna Vehkamäki, Albert Viggiano and many others for helpful discussions as well as Bärbel Langmann and Angelika Heil for critically reviewing the manuscript.

The service charges for this open access publication
have been covered by the Max Planck Society.

References

Adams, P. J. and Seinfeld, J. H.: Predicting global aerosol size distributions in general circulation models, J. Geophys. Res., 107(D19), 4370, doi:10.1029/2001JD001010, 2002. 1363, 1387

Andres, R. J. and Kasgnoc, A. D.: A time-averaged inventory of subaerial volcanic sulfur emissions, J. Geophys. Res., 103, 25251–25261, 1998. 1369

Angell, J. K., Korshover, J., and Planet, W. G.: Ground-based and satellite evidence for a pronounced total-ozone minimum in early 1983 and responsible atmospheric layers, Mon. Weather Rev., 113, 641–646, 1985. 1361

Arnold, F. and Fabian, R.: First measurements of gas phase sulphuric acid in the stratosphere, Nature, 283, 55–57, 1980. 1377, 1411

Arnold, F. and Qiu, S.: Upper stratosphere negative ion composition measurements and inferred trace gas abundances, Planet. Space Sci., 32, 169–177, 1984. 1377, 1411

Arnold, F., Fabian, R., and Joos, W.: Measurements of the height variation of sulfuric acid vapor concentrations in the stratosphere, Geophys. Res. Lett., 8, 293–296, 1981. 1377, 1411

Baldwin, M. P., Gray, L. J., Dunkerton, T. J., Hamilton, K., Haynes, P. H., Randel, W. J., Holton, J. R., Alexander, M. J., Hirota, I., Horinouchi, T., Jones, D. B. A., Kinnersley, J. S., Marquardt, C., Sato, K., and Takahashi, M.: The quasi-biennial oscillation, Rev. Geophys., 39, 179–229, 2001. 1382

Bannister, R. N., O'Neil, A., Gregory, A. R., and Nissen, K. M.: The role of the south-east Asian monsoon and other seasonal features in creating the "tape-recorder" signal in the Unified Model, Q. J. Roy. Meteor. Soc., 130, 1531–1554, 2004. 1383

Barth, M. C., Rasch, P. J., Kiehl, J. T., Benkovitz, C. M., and Schwartz, S. E.: Sulfur chemistry in the National Center for Atmospheric Research Community Climate Model: Description, evaluation, features, and sensitivity to aqueous chemistry, J. Geophys. Res., 105, 1387–1415, 2000. 1407

Bauman, J. J., Russell, P. B., Geller, M. A., and Hamill, P.: A stratospheric aerosol climatology from SAGE II and CLAES measurements: 1. Methodology, J. Geophys. Res., 108, 4382, doi:10.1029/2002JD002992, 2003a. 1370, 1408, 1417

Bauman, J. J., Russell, P. B., Geller, M. A., and Hamill, P.: A stratospheric aerosol climatology from SAGE II and CLAES measurements: 2. Results and comparisons, 1984–1999, J. Geophys. Res., 108, 4383, doi:10.1029/2002JD002993b. 1370, 1371, 1408, 1417

Baumgardner, D., Kok, G., and Raga, G.: Warming of the Arctic lower stratosphere by light absorbing particles, Geophys. Res. Lett., 31, L06117, doi:10.1029/2003GL018883, 2004. 1361

Bekki, S. and Pyle, J.: Two-dimensional assessment of the impact of aircraft sulphur emissions on the stratospheric sulfate aerosol layer, J. Geophys. Res., 97, 15839–15847, 1992. 1364

Borrmann, S., Solomon, S., Dye, J. E., Baumgardner, D., Kelly, K. K., and Chan, K. R.: Heterogeneous reactions on stratospheric background aerosols, volcanic sulfuric acid droplets, and type I polar stratospheric clouds: Effects of temperature fluctuations and differences in particle phase, J. Geophys. Res, 102, 3639–3648, 1997. 1361

Brock, C. A., Hamill, P., Wilson, J. C., Jonsson, H. H., and Chan, K. R.: Particle formation in the upper tropical troposphere: A source of nuclei for the stratospheric aerosol, Science, 270, 1650–1653, 1995. 1383

Burkholder, J. B. and McKeen, S.: UV absorption cross sections for SO_3, Geophys. Res. Lett., 24, 3201–3204, 1997. 1378

Chin, M., Jacob, D., Gardner, G., Foreman-Fowler, M., Spiro, P., and Savoie, D.: A global threedimensional model of tropospheric sulfate, J. Geophys. Res., 101, 18667–18690, 1996. 1374

Crutzen, P. J.: Albedo enhancement by stratospheric sulfur injections: A contribution to resolve a policy dilemma?, Climatic Change, 77, 211–219, 2006. 1361

Dameris, M., Grewe, V., Ponater, M., Deckert, R., Eyring, V., Mager, F., Matthes, S., Schnadt, C., Stenke, A., Steil, B., Brühl, C., and Giorgetta, M. A.: Long-term changes and variability in a transient simulation with a chemistry-climate model employing realistic forcing, Atmos. Chem. Phys., 5, 2121–2145, doi:10.5194/acp-5-2121-2005, 2005. 1369

DeMott, P., D.J. Cziczo, D., Prenni, A., Murphy, D., Kreidenweis, S., Thomson, D., Borys, R., and Rogers, D.: Measurements of the concentration and composition of nuclei for cirrus formation, P. Natl. Acad. Sci. USA, 100, 14655–14660, 2003. 1361

Dentener, F., Kinne, S., Bond, T., Boucher, O., Cofala, J., Generoso, S., Ginoux, P., Gong, S., Hoelzemann, J. J., Ito, A., Marelli, L., Penner, J. E., Putaud, J.-P., Textor, C., Schulz, M., van der Werf, G. R., and Wilson, J.: Emissions of primary aerosol and precursor gases in the years 2000 and 1750 prescribed data-sets for AeroCom, Atmos. Chem. Phys., 6, 4321–4344, doi:10.5194/acp-6-4321-2006, 2006. 1368

Deshler, T., Hervig, M. E., Hofmann, D. J., Rosen, J. M., and Liley, J. B.: Thirty years of in situ stratospheric aerosol size distribution measurements from Laramie, Wyoming (41° N), using balloon-borne instruments, J. Geophys. Res., 108, 4167, doi:10.1029/2002JD002514, 2003a. 1363, 1371, 1372, 1389, 1391, 1419, 1421

Deshler, T., Larsen, N., Weissner, C., Schreiner, J., Mauersberger, K., Cairo, F., Adriani, A., Donfrancesco, G. D., Ovarlez, J., Ovarlez, H., Blum, U., Fricke, K., and Dörnbrack, A.: Large nitric acid particles at the top of an Arctic stratospheric cloud, J. Geophys. Res., 108(D16), 4517, doi:10.1029/2003JD003479, 2003b. 1361

Deshler, T., Anderson-Sprecher, R., Jäger, H., Barnes, J., Hofmann, D. J., Clemesha, B., Simonich, D., Osborn, M., Grainger, R. G., and Godin-Beekmann, S.: Trends in the nonvolcanic component of stratospheric aerosol over the period 1971–2004, J. Geophys. Res., 111, D01201, doi:10.1029/2005JD006089, 2006. 1371

Dubovik, O., Smirnov, A., Holben, B. N., King, M. D., Kaufman, Y. J., Eck, T. F., and Slutsker, I.: Accuracy assessments of aerosol optical properties retrieved from Aerosol Robotic Network

(AERONET) Sun and sky radiance measurements, J. Geophys. Res., 105, 9791–9806, 2000. 1363, 1386

Dusek, U., Frank, G. P., Hildebrandt, L., Curtius, J., Schneider, J., Walter, S., Chand, D., Drewnick, F., Hings, S., Jung, D., Borrmann, S., and Andreae, M. O.: Size Matters More Than Chemistry for Cloud-Nucleating Ability of Aerosol Particles, Science, 312, 1375–1378, doi:10.1126/science.1125261, 2006. 1363

Easter, R. C., Ghan, S. J., Zhang, Y., Saylor, R. D., Chapman, E. G., Laulainen, N. S., Abdul-Razzak, H., Leung, L. R., Bian, X., and Zaveri, R. A.: MIRAGE: Model description and evaluation of aerosols and trace gases, J. Geophys. Res., 109, D20210, doi:10.1029/2004JD004571, 2004. 1382, 1407

Feichter, J., Kjellstrom, E., Rohde, H., Dentener, F., Lelieveld, J., and Roelofs, G. J.: Simulation of the tropospheric sulfur cycle in a global climate model, Atmos. Environ., 30, 1693–1707, 1996. 1369, 1407

Fouquart, Y. and Bonnel, B.: Computations of solar heating of the earth's atmosphere: A new parameterisation, Beitr. Phys. Atmos., 53, 35–62, 1980. 1366

Froyd, K. D., Murphy, D. M., Sanford, T. J., Thomson, D. S., Wilson, J. C., Pfister, L., and Lait, L.: Aerosol composition of the tropical upper troposphere, Atmos. Chem. Phys., 9, 4363–4385, doi:10.5194/acp-9-4363-2009, 2009. 1361

Fu, R., Hu, Y., Wright, J. W., et al.: Short circuit of water vapor and polluted air to the global stratosphere by convective transport over the Tibetan Plateau, P. Natl. Acad. Sci. USA, 103, 5664–5669, 2006. 1383

Fueglistaler, S., Dessler, A. E., Dunkerton, T. J., Folkins, I., Fu, Q., and Mote, P. W.: Tropical tropopause layer, Rev. Geophys., 47, RG1004, doi:10.1029/2008RG000267, 2009. 1383

Gelbard, F., Tambour, Y., and Seinfeld, J. H.: Sectional representations for simulating aerosol dynamics, J. Colloid Interf. Sci., 76, 541–556, 1980. 1367

Gerding, M., Baumgarten, G., Blum, U., Thayer, J. P., Fricke, K.-H., Neuber, R., and Fiedler, J.: Observation of an unusual mid-stratospheric aerosol layer in the Arctic: Possible sources and implications for polar vortex dynamics, Annales Geophys., 21, 1057–1069, 2003. 1361

Ghan, S. J. and Schwartz, S. E.: Aerosol properties and processes: A path from field and laboratory measurements to global climate models, B. Am. Meteorol. Soc., 88(7), 1059–1083, doi:10.1175/BAMS-88-7-1059, 2007. 1364

Grainger, R., Lambert, A., rogers, C., Taylor, F., and Deshler, T.: Straospheric aerosol effective radius, surface area and volume estimated from infrared measurements, J. Geophys. Res.,

100, 16507–16518, 1995. 1387
Halmer, M. M., Schmincke, H.-U., and Graf, H.-F.: The annual volcanic gas input into the atmosphere, in particular into the stratosphere: A global data set for the past 100 years, J. Volcanol. Geoth. Res., 115, 511–528, 2002. 1369
Hamill, P., Toon, O. B., and Kiang, C. S.: Microphysical processes affecting stratospheric aerosol particles, J. Atmos. Sci., 34, 1104–1119, 1977. 1367
Hamill, P., Jensen, E. J., Russel, P. B., and Bauman, J. J.: The life cycle of stratospheric aerosol particles, B. Am. Meteorol. Soc., 78, 1395–1410, 1997. 1362
Heckendorn, P., Weisenstein, D., Fueglistaler, S., Luo, B. P., Rozanov, E., Schraner, M., Thomason, L. W., and Peter, T.: The impact of geoengineering aerosols on stratospheric temperature and ozone, Environ. Res. Lett., 4, 045108, doi:10.1088/1748-9326/4/4/045108, 2009. 1361, 1364
Heitmann, H. and Arnold, F.: Composition measurements of troposheric ions, Nature, 306, 747–751, 1983. 1377, 1411
Hines, C. O.: Doppler-spread parameterization of gravity wave momentum deposition in the middle atmosphere, 2, Broad and quasi-monochromatic spectra, and implementation, J. Atmos. Terr. Phys., 59, 387–400, 1997. 1366
Hitchman, M. H., McKay, M., and Trepte, C. R.: A climatology of stratospheric aerosol, J. Geophys. Res., 99, 20689–20700, 1994. 1362, 1382
Hofmann, D., Rosen, J., Harder, J., and Hereford, J.: Balloon-Borne Measurements of Aerosol, Condensation nuclei, and cloud particles in the stratosphere at McMurdo station, Antarctica, during the spring of 1987, J. Geophys. Res., 94, 11253–11269, 1989. 1385
Holton, J. R., Haynes, P. H., McIntyre, M. E., Douglass, A. R., Rood, R. R., and Pfister, L.: Stratospheric-tropospheric exchange, Rev. Geophys., 33, 403–439, 1995. 1362
Hommel, R.: Die Variabilität von stratosphärischem Hintergrund-Aerosol, Eine Untersuchung mit dem globalen sektionalen Aerosolmodell MAECHAM5-SAM2, Ph.D. thesis, Universität Hamburg, 2008 (in German). 1368, 1373
Hommel, R. and Graf, H.-F.: Modelling the size distribution of geoengineered stratospheric aerosols, Atmos. Sci. Lett., in press, doi:10.1002/asl.285, 2010. 1376
Hommel, R., Timmreck, C., Giorgetta, M. A., and Graf, H.-F.: The interannual variability of the background stratospheric aerosol layer, Geosci. Model Dev. Discuss., in preperation, 2010. 1386
Horowitz, L. W., Walters, S., Mauzerall, D. L., Emmons, L. K., Rasch, P. J., Granier, C., Tie,

X. X., Lamarque, J. F., Schultz, M. G., Orlando, G. S., and Brasseur, G. P.: A global simulation of tropospheric ozone and related tracers: Description and evaluation of MOZART, Version 2, J. Geophys. Res., 108, 4784, doi:10.1029/2002JD002853, 2003. 1369

Hunton, D., Ballenthin, J. O., Borghetti, J. F., et al.: Chemical ionization mass spectrometric measurements of SO_2 emissions from jet engines in flight and test chamber operations, J. Geophys. Res., 105, 26841–26855, 2000. 1372

IPCC: Climate Change 2007: The Physical Science Basis, in: Contribution of Working Group I to the Fourth Assessment Report of the Intergovernmental Panel on Climate Change, edited by: Solomon, S., Qin, D., Manning, M., Chen, Z., Marquis, M., Averyt, K. B., Tignor, M., and Miller, H. L., Cambridge University Press, Cambridge, United Kingdom and New York, NY, USA, 996 pp., 2007. 1361, 1364

Jacobson, M. Z.: Development and application of a new air pollution modelling system – Part II. Aerosol module structure and design, Atmos. Environ., 31, 131–144, 1997. 1390

Jöckel, P., Sander, R., Kerkweg, A., Tost, H., and Lelieveld, J.: Technical Note: The Modular Earth Submodel System (MESSy) – a new approach towards Earth System Modeling, Atmos. Chem. Phys., 5, 433–444, doi:10.5194/acp-5-433-2005, 2005. 1369

JPL/NASA: Chemical Kinetics and Photochemical Data for Use in Atmospheric Studies, JPL Publication 02-25, Evaluation No 14, edited by: Sander, S. P., Friedl, R. R., Ravishankara, A. R., Golden, D. M., Kolb, C. E., Kurylo, M. J., Huie, R. E., Orkin, V. L., Molina, M. J., Moortgat, G. K., and Finlayson-Pitts, B. J., NASA Jet Propulsion Laboratory, California Institute of Technology, Pasadena, California, 2003. 1406

Kent, G., Wang, P.-H., McCormick, M., and Skeens, K.: Multiyear Stratospheric Aerosol and Gas Experiment II measurements of upper tropospheric aerosol characteristics, J. Geophys. Res., 100, 13875–13899, 1995. 1371, 1388, 1408

Kent, G. S. and McCormick, M. P.: SAGE and SAM-II measurements of global stratospheric aerosol optical depth and mass loading, J. Geophys. Res., 84, 5303–5314, 1984. 1362, 1374

Kettle, A. and Andreae, M.: Flux of the dimethylsulfide from the oceans: A comparison of updated data sets and flux models, J. Geophys. Res., 105, 26793–26808, 2000. 1369

Kloster, S., Feichter, J., Maier-Reimer, E., Six, K. D., Stier, P., and Wetzel, P.: DMS cycle in the marine ocean-atmosphere system - a global model study, Biogeosciences, 3, 29–51, doi:10.5194/bg-3-29-2006, 2006. 1369, 1374, 1375, 1407

Kokkola, H., Hommel, R., Kazil, J., Niemeier, U., Partanen, A.-I., Feichter, J., and Timmreck, C.:

Aerosol microphysics modules in the framework of the ECHAM5 climate model - intercomparison under stratospheric conditions, Geosci. Model Dev., 2, 97–112, doi:10.5194/gmd-2-97-2009, 2009. 1368, 1375, 1386

Lacis, A., Hansen, J., and Sato, M.: Climate forcing by stratospheric aerosols, Geophys. Res. Lett., 19, 1607–1610, 1992. 1361

Lee, S.-H., Reeves, J. M., Wilson, J. C., Hunton, D. E., Viggiano, A. A., Miller, T. M., Ballenthin, J. O., and Lait, L. R.: Particle formation by ion nucleation in the upper troposphere and lower stratosphere, Science, 301, 1886–1889, 2003. 1372, 1379, 1412

Lin, S. J. and Rood, R. B.: Multidimensional flux form semi-Lagrangian transport, Mon. Weather Rev., 124, 2046–2068, 1996. 1366

Liu, X., E., P. J., and M., H.: Global modeling of aerosol dynamics: Model description, evaluation, and interactions between sulfate and nonsulfate aerosols, J. Geophys. Res., 110, D18206, doi:10.1029/2004JD005674, 2005. 1375, 1407

Ma, X. and von Salzen, K.: Dynamics of the sulphate aerosol size distribution on a global scale, J. Geophys. Res., 111, D08206, doi:10.1029/2005JD006620, 2006. 1381, 1382

Makkonen, R., Asmi, A., Korhonen, H., Kokkola, H., Järvenoja, S., Räisänen, P., Lehtinen, K. E. J., Laaksonen, A., Kerminen, V.-M., Järvinen, H., Lohmann, U., Bennartz, R., Feichter, J., and Kulmala, M.: Sensitivity of aerosol concentrations and cloud properties to nucleation and secondary organic distribution in ECHAM5-HAM global circulation model, Atmos. Chem. Phys., 9, 1747–1766, doi:10.5194/acp-9-1747-2009, 2009. 1382, 1389

Manzini, E., Giorgetta, M. A., Esch, M., Kornblueh, L., and Roeckner, E.: The influence of sea surface temperatures on the northern winter stratosphere: Ensemble simulations with the MAECHAM5 model, J. Climate, 19, 3863–3881, 2006. 1366

McCormick, M. P.: SAGE II: an overview, Adv. Space Res., 7, 219–226, 1987. 1370

McIntyre, M. E. and Palmer, T. N.: The “surf zone” in the stratosphere, J. Atmos. Terr. Phys., 46, 825–849, 1984. 1386

Meixner, F. X.: The vertical sulfur dioxide distribution at the tropopause level, J. Atmos. Chem., 2, 175–189, 1984. 1377

Mills, M., Toon, O. B., and Solomon, S.: A 2D microphysical model of the polar stratospheric CN layer, Geophys. Res. Lett., 26, 1133–1136, 1999. 1365, 1384

Mills, M., Toon, O., Vaida, V., Hintze, P., Kjaergaard, H., Schofield, D., and Robinson, T.: Photolysis of sulfuric acid vapor by visible light as a source of the polar stratospheric CN layer, J. Geophys. Res., 110, doi:10.1029/2004JD005519, 2005a. 1362, 1365, 1370, 1379, 1384,

1411
Mills, M., Toon, O., Vaida, V., Hintze, P., Kjaergaard, H., Schofield, D., and Robinson, T.: Photolysis of sulfuric acid vapor by visible light as a source of the polar stratospheric CN layer, J. Geophys. Res., 110, doi:10.1029/2004JD005519, 2005b. 1362, 1365, 1378
Mlawer, E. J., Taubman, S. J., Brown, P. D., Iacono, M. J., and Clough, S. A.: Radiative transfer for inhomogeneous atmospheres: RRTM, a validated correlated-k model for the longwave, J. Geophys. Res., 102, 16663–16682, 1997. 1366
Möhler, O. and Arnold, F.: Gaseous sulfuric acid and sulfur dioxide measurements in the arctic troposphere and lower stratosphere: Implications for hydroxyl radical abundances, Geophys. Res. Lett., 19, 1763–1766, 1992. 1377
Myhre, G., Stordal, F., Berglen, T., Sundet, J., and Isaksen, I.: Uncertainties in the Radiative Forcing Due to Sulfate Aerosols, J. Atmos. Sci., 61, 485–498, doi:10.1175/1520-0469(2004)061⟨0485:UITRFD⟩2.0.CO;2, 2004. 1364
Pan, W., Tatang, M., McRae, G., and Prinn, R.: Uncertainty analysis of indirect radiative forcing by anthropogenic sulfate aerosols, J. Geophys. Res., 103, 3815–3823, 1998. 1364
PARTS: Particles in the upper troposphere and lower stratosphere and their role in the climate system (PARTS): Detailed report, related to overall project duration, edited by: Graf, H.-F., European Commission, European Research Framework 5, available at: http://parts.dkrz.de (last access: September 2010), 2004. 1370
Penner, J., Andreae, M., Annegarn, H., Barrie, L., Feichter, J., Hegg, D., Jayaraman, A., Leaitch, R., Murphy, D., Nganga, J., and Pitari, G.: Climate Change 2001: The Scientific Basis, in: Chapter 5: Aerosols, their Direct and Indirect Effects, IPCC Third Assessment Report, Cambridge University Press, Cambridge, United Kingdom and New York, NY, USA, 996 pp., 2001. 1375
Pham, M., Muller, J.-F., Brasseur, G., Granier, C., and Megie, G.: A three-dimensional study of the tropospheric sulfur cycle, J. Geophys. Res., 100, 26061–26092, 1995. 1369, 1375
Pinnick, R. G., Rosen, J. M., and Hofmann, D. J.: Stratospheric aerosol measurements, 3, Optical model calculations, J. Atmos. Sci., 33, 304–314, 1976. 1373, 1391
Pitari, G., Mancini, E., Rizi, V., and Shindell, D. T.: Impact of future climate and emission changes on stratospheric aerosols and ozone, J. Atmos. Sci., 59, 414–440, 2002. 1362, 1364, 1365, 1374, 1386
Rasch, P. J., Crutzen, P. J., and Coleman, D. B.: Exploring the geoengineering of climate using stratospheric sulfate aerosols: The role of particle size, Geophys. Res. Lett., 35, L02809,

doi:10.1029/2007GL032179, 2008. 1361, 1363, 1364
Reiner, T. and Arnold, F.: Stratospheric SO_3: Upper limits inferred from ion composition measurements – Implications for H_2SO_4 and aerosol formation, Geophys. Res. Lett., 24, 1751–1754, 1997. 1377, 1411
Rinsland, C. P., Gunson, M. R., Ko, M. K. W., Weisenstein, D. W., Zander, R., Abrams, M. C., Goldman, A., Sze, N. D., and Yue, G. K.: H_2SO_4 photolysis: A source of sulfur dioxide in the upper stratosphere, Geophys. Res. Lett., 22, 1109–1112, 1995. 1362, 1370, 1377, 1379, 1411
Robock, A.: Volcanic eruptions and climate, Rev. Geophys., 38, 191–219, 2000. 1361
Roche, A. E., Kumer, J. B., Mergenthaler, J. L., Ely, G. A., Uplinger, W. G., Potter, J. F., James, T. C., and Sterritt, L. W.: The Cryogenic Limb Array Etalon Spectrometer (CLAES) on UARS: Experiment Description and Performance., J. Geophys. Res., 98, 10763–10775, doi:10.1029/93JD00800, 1993. 1371
Roeckner, E., Baueml, G., Bonaventura, L., Brokopf, R., Esch, M., Giorgetta, M., Hagemann, S., Kirchner, I., Kornblueh, L., Manzini, E., Rhodin, A., Schlese, U., Schulzweida, U., and Tompkins, A.: The atmospheric general circulation model ECHAM5 – Part I, MPI Report No. 349, 2003. 1366
Rose, W., Gu, Y., Watson, I., Yu, T., Bluth, G., Prata, A., Krueger, A., Krotkov, N., Carn, S., Fromm, M., Hunton, D., Ernst, G., Viggiano, A., Miller, T., Ballentin, J., Reeves, J., Wilson, J., Anderson, B., and Flittner, D.: The February–March 2000 eruption of Hekla, Iceland from a satellite perspective, in: AGU Geophysical Monograph 139: Volcanism and the Earth's Atmosphere, ISBN 0-87590-998-1, edited by: Robock, A. and Oppenheimer, C., John Wiley and Sons, 107–132, 2003. 1372, 1378
Russell, P. B., Livingston, J. M., Pueschel, R. F., Pollack, J. B., Brooks, S., Hamill, P., Hughes, J., Thomason, L., Stowe, L., Deshler, T., and Dutton, E.: Global to microscale evolution of the Pinatubo volcanic aerosol, derived from diverse measurements and analyses, J. Geophys. Res., 101, 18745–18763, 1996. 1363
Schlager, H. and Arnold, F.: Balloon-borne composition measurements of stratospheric negative ions and inferred sulfuric acid vapor abundances during the MAP/GLOBUS 1983 campaign, Planet. Space Sci., 35, 693–701, 1987. 1377, 1411
Seinfeld, J. H. and Pandis, S. N.: Atmospheric chemistry and physics: From air pollution to climate change, Wiley-Interscience, New York, 1998. 1367
Sheridan, P. J., Brock, C. A., and Wilson, J. C.: Aerosol particles in the upper troposphere

GMDD
3, 1359–1421, 2010

and lower stratosphere: Elemental composition and morphology of individual particles in northern mid-latitudes, Geophys. Res. Lett., 21, 2587–2590, 1994. 1361

SPARC/ASAP: WMO/SPARC Scientific Assessment of Stratospheric Aerosol Properties (ASAP), WCRP-124 WMO/TD-No. 1295, SPARC Report No. 4, edited by: Thomason, L. and Peter, Th., WMO, 2006. 1360, 1361, 1362, 1363, 1365, 1369, 1370, 1371, 1372, 1374, 1375, 1376, 1377, 1379, 1380, 1384, 1388, 1391, 1408

Spracklen, D. V., Pringle, K. J., Carslaw, K. S., Chipperfield, M. P., and Mann, G. W.: A global off-line model of size-resolved aerosol microphysics: I. Model development and prediction of aerosol properties, Atmos. Chem. Phys., 5, 2227–2252, doi:10.5194/acp-5-2227-2005, 2005. 1363, 1382

Steele, H., Lumpe, J., Turco, R., Bevilacqua, R., and Massie, S.: Retrieval of aerosol surface area and volume densities from extinction measurements: Application to POAM II and SAGE II, J. Geophys. Res., 104, 9325–9336, 1999. 1371

Steele, H. M. and Hamill, P.: Effects of temperature and humidity on the growth and optical properties of sulfuric acid-water droplets in the stratosphere, J. Aerosol Sci., 12, 517–528, 1981. 1367

Steil, B., Brühl, C., Manzini, E., Crutzen, P. J., Lelieveld, J., Rasch, P. J., Roeckner, E., and Krueger, K.: A new interactive chemistry-climate model. 1. Present day climatology and interannual variability of the middle atmosphere using the model and 9 years of HALOE/UARS data, J. Geophys. Res., 108(D9), 4290, doi:10.1029/2002JD002971, 2003. 1369

Stenchikov, G., Robock, A., Ramaswamy, V., Schwartzkopf, M. D., Hamilton, K., and Ramachandran, S.: Arctic Oscillation response to the 1991 Mount Pinatubo eruption: Effects of volcanic aerosols and ozone depletion, J. Geophys. Res, 107, 1–16, 2002. 1362

Stenchikov, G., Hamilton, K., Stouffer, R. J., Robock, A., Ramaswamy, V., Santer, B., and Graf, H.-F.: Arctic Oscillation response to volcanic eruptions in the IPCC AR4 climate models, J. Geophys. Res., 111, D07107, doi:10.1029/2005JD006286, 2006. 1362

Stier, P., Feichter, J., Kinne, S., Kloster, S., Vignati, E., Wilson, J., Ganzeveld, L., Tegen, I., Werner, M., Balkanski, Y., Schulz, M., Boucher, O., Minikin, A., and Petzold, A.: The aerosol-climate model ECHAM5-HAM, Atmos. Chem. Phys., 5, 1125–1156, doi:10.5194/acp-5-1125-2005, 2005. 1363, 1368, 1374, 1375, 1381, 1382, 1407

Takigawa, M., Takahashi, M., and Akiyoshi, H.: Simulation of stratospheric sulfate aerosols using a Center for Climate System Research/National Institute for Environmental Studies atmospheric GCM with coupled chemistry 1. Nonvolcanic simulation, J. Geophys. Res., 107(D22),

GMDD
3, 1359–1421, 2010

4610, doi:10.1029/2001JD001007, 2002. 1362, 1363, 1364, 1374, 1376, 1380

Tanre, D., Geleyn, J.-F., and Slingo, J. M.: First results of the introduction of an advanced aerosol-radiation interaction in the ECMWF low resolution global model, in Aerosols and Their Climatic Effects, edited by: Gerber, H. and Deepak, A., Hampton, VA, 133–177, 1984. 1366

Thomas, M. A., Timmreck, C., Giorgetta, M. A., Graf, H.-F., and Stenchikov, G.: Simulation of the climate impact of Mt. Pinatubo eruption using ECHAM5 - Part 1: Sensitivity to the modes of atmospheric circulation and boundary conditions, Atmos. Chem. Phys., 9, 757–769, doi:10.5194/acp-9-757-2009, 2009. 1362

Thomason, L. W., Poole, L. R., and Deshler, T.: A global climatology of stratospheric aerosol surface area density deduced from Stratospheric Aerosol and Gas Experiments II measurements: 1984–1994, J. Geophys. Res., 102, 8967–8976, 1997. 1371

Thomason, L. W., Burton, S. P., Luo, B.-P., and Peter, T.: SAGE II measurements of stratospheric aerosol properties at non-volcanic levels, Atmos. Chem. Phys., 8, 983–995, doi:10.5194/acp-8-983-2008, 2008. 1360, 1386, 1391

Timmreck, C.: Three-dimensional simulation of stratospheric background aerosol: First results of a multiannual general circulation model simulation, J. Geophys. Res., 106, 28313–28332, 2001. 1363, 1364, 1365, 1367, 1383, 1408

Timmreck, C. and Graf, H.-F.: A microphysical model to simulate the development of stratospheric aerosol in a GCM, Meteorol. Z., 9, 263–282, 2000. 1367, 1368

Timmreck, C., Graf, H.-F., and Kirchner, I.: A one and half year interactive MA/ECHAM4 simulation of Mount Pinatubo Aerosol, J. Geophys. Res., 104, 9337–9360, 1999. 1364

Tolbert, M. A.: Sulfate aerosols and polar stratospheric cloud formation, Science, 264, 527–528, 1994. 1361

Toon, O. B., Turco, R. P., Hamill, P., Kiang, C. S., and Whitten, R. C.: A one-dimensional model describing aerosol formation and evolution in the stratosphere: II. Sensitivity studies and comparision with observations, J. Atmos. Sci., 36, 718–736, 1979. 1380

Trepte, C. R. and Hitchman, M. H.: Tropical stratospheric circulation deduced from satellite aerosol data, Nature, 355, 626–628, 1992. 1362, 1382

Tsang, T. H. and Brock, J. R.: Simulation of condensation aerosol growth by condensation and evaporation, Aerosol Sci. Tech., 2, 311–320, 1983. 1368

Turco, R. P., Hamill, P., Toon, O. B., Whitten, R. C., and Kiang, C. S.: A one-dimensional model describing aerosol formation and evolution in the stratosphere: I. physical processes and

mathematical analogs, J. Atmos. Sci., 36, 699–717, 1979. 1364, 1370, 1380
Turco, R. P., Toon, O. B., Hamill, P., and Whitten, R. C.: Effects of meteoric debris on stratospheric aerosols and gases, J. Geophys. Res., 86, 1113–1128, 1981. 1378
Vaida, V., Kjaergaard, H. G., Hintze, P. E., and Donaldson, D. J.: Photolysis of sulfuric acid vapor by visible solar radiation, Science, 299, 1566–1568, 2003. 1362, 1370
Vehkamäki, H., Kulmala, M., Napari, I., Lehtinen, K. E. J., Timmreck, C., Noppel, M., and Laaksonen, A.: An improved parameterization for sulfuric acid water nucleation rates for tropospheric and stratospheric conditions, J. Geophys. Res., 107, 4622–4632, 2002. 1368
Viggiano, A. A. and Arnold, F.: Extended sulfuric acid vapor concentration measurements in the stratosphere, Geophys. Res. Lett., 8, 583–586, 1981. 1377, 1411
Waugh, D. W., Plumb, R. A., Newman, P. A., Schoeberl, M. R., Lait, L. R., Loewenstein, M., Podolske, J. R., Elkins, J. W., and Chan, K. R.: Fine-scale, poleward transport of tropical air during AASE 2, Geophys. Res. Lett., 21, 2603–2606, 1994. 1385
Weisenstein, D. K., Yue, G. K., Ko, M. K. W., Sze, N.-D., Rodriguez, J. M., and Scott, C. J.: A two-dimensional model of sulfur species and aerosols, J. Geophys. Res., 102, 13019–13035, 1997. 1364, 1374, 1375, 1376, 1377, 1380, 1383, 1388, 1408
Weisenstein, D. K., Penner, J. E., Herzog, M., and Liu, X.: Global 2-D intercomparison of sectional and modal aerosol modules, Atmos. Chem. Phys., 7, 2339–2355, doi:10.5194/acp-7-2339-2007, 2007. 1375, 1408
Wurl, D., Grainger, R. G., McDonald, A. J., and Deshler, T.: Optimal estimation retrieval of aerosol microphysical properties from SAGE II satellite observations in the volcanically unperturbed lower stratosphere, Atmos. Chem. Phys., 10, 4295–4317, doi:10.5194/acp-10-4295-2010, 2010. 1360, 1363, 1370, 1371, 1408, 1417
Yue, G., Poole, L., Wang, P.-H., and Chiou, E.: Stratospheric aerosol acidity, density, and refractive index deduced from SAGE II and NMC temperature data, J. Geophys. Res., 99, 3727–3738, 1994. 1388, 1408
Zhang, Y., Easter, R. C., Ghan, S. J., and Abdul-Razzak, H.: Impact of aerosol size representation on modelling aerosol-cloud interactions, J. Geophys. Res., 107(D21), 4558, doi:10.1029/2001JD001549, 2002. 1363, 1364
Zhao, J. and Turco, R. P.: Nucleation simulation in the wake of a jet aircraft in stratospheric flight, J. Atmos. Sci., 26, 779–795, 1995. 1384

GMDD
3, 1359–1421, 2010

Table 1. Reactions and reaction rate coefficients of stratospheric sulphur chemistry in MAECHAM5-SAM2. Intermediate reactions bypassed where products are given in brackets. Reaction rate constants after JPL/NASA (2003).

Homogeneous reactions in the stratosphere			
Reaction			Reaction rate [$cm^{-3}\,s^{-1}$]
$SO + O_2$	$\rightarrow$	$SO_2 + O$	$R_2 = 2.6 \times 10^{-13} e^{-2400/T}$
$SO + O_3$	$\rightarrow$	$SO_2 + O_2$	$R_8 = 2.6 \times 10^{-13} e^{-2400/T}$
$SO + NO_2$	$\rightarrow$	$SO_2 + NO$	$R_1 = 1.4 \times 10^{-11}$
$SO_2 + O$	$\rightarrow$	SO_3	$R_{10} = f(K_0), \quad K_0 = 1.3 \times 10^{-33}(T/300)^{-3.6}$
$SO_2 + O_3$	$\rightarrow$	$SO_3 + O_2$	$R_9 = 3.0 \times 10^{-12} e^{-7000/T}$
$SO_2 + OH$	$\rightarrow$	$HOSO_2$	$R_5 = f(K_0, K_\infty), K_0 = 3.0 \times 10^{-31}(T/300)^{-3.3}$, $K_\infty = 1.5 \times 10^{-12}$
$SO_3 + H_2O$	$\rightarrow$	(H_2SO_4)	$R_7 = 2.26 \times 10^{-43} \cdot T \cdot e^{6544/T} \cdot H_2O$
$HOSO_2 + O_2$	$\rightarrow$	$SO_3 + HO_2$	$R_6 = 1.3 \times 10^{-12} e^{-330/T}$
$OCS + O$	$\rightarrow$	$SO + CO$	$R_3 = 2.1 \times 10^{-11} e^{-2200/T}$
$OCS + OH$	$\rightarrow$	$(SO_2 + CO_2)$	$R_4 = 1.1 \times 10^{-13} e^{-1200/T}$
Photolysis Reaction			
$OCS + hv$	$\rightarrow$	$CO + S$	
$H_2SO_4 + hv$	$\rightarrow$	$SO_3 + H_2O$	
$SO_2 + hv$	$\rightarrow$	$SO + O$	
$SO_3 + hv$	$\rightarrow$	$SO_2 + O$	
$O_3 + hv$	$\rightarrow$	$O_2 + O$	

GMDD
3, 1359–1421, 2010

Table 2. Comparison of sulphate aerosol burden and lifetimes from this and other climate model studies.

	Burden [Tg(s)]	Lifetime [d]
MAECHAM5-SAM2	0.88	4.25
Stier et al. (2005)*	0.8	3.9
Kloster et al. (2006)*	0.73	3.42
Feichter et al. (1996)**	0.57	4.3
Barth et al. (2000)	0.57	3.8
Easter et al. (2004)	1.07	6.8
Liu et al. (2005)	0.89	2.6

* ECHAM5-HAM,
** ECHAM4 incl. tropospheric sulphur cycle.

GMDD
3, 1359–1421, 2010

Table 3. Stratospheric aerosol mass densities in [$\mu g\,m^{-3}$] at 40° N and three altitudes, derived from different models and oberservations. Models: [1] This work, 3-D, MAECHAM5, 35 bins; [2] Timmreck (2001), 3-D, ECHAM4, 35 bins; [3] Weisenstein et al. (1997), 2-D, 40 bins; [4] SPARC/ASAP (2006), 2-D, 40 bins, and [5] Weisenstein et al. (2007), 2-D, 150 bins. SAGE II: [6] Wurl et al. (2010); [7] Bauman et al. (2003a,b); [8] Yue et al. (1994); and [9] Kent et al. (1995). Data for OPC and PCAS (*Passive Cavity Aerosol Spectrometer*) are also taken from Kent et al. (1995).

	Models				
	SAM2[1] Mean 1998	SAM[2] Annual mean	AER40[3] Mean April	AER40[4] Annual mean	AER150[5] Annual mean
24 km	0.03	0.05	0.05	0.04	0.04
21 km	0.08	0.08	0.07	0.08	0.07
16 km	0.12	0.10	0.13	0.17	0.13

	SAGE II				OPC/PCAS
	UOX[6] Mean 1998	AMES[7] Mean 1998	Yue et al.[8] Mean Apr 1991	Kent et al.[9] Mean Pre-Pinatubo 1988–Apr 1991	Kent et al.[9] Mean Pre-Pinatubo 1988–Apr 1991
24 km	0.04	0.03	~0.05	0.05–0.1	–
21 km	0.07	0.08	~0.08	0.19	0.1
16 km	0.11	0.12	~0.13	0.19	0.03–0.06

GMDD
3, 1359–1421, 2010

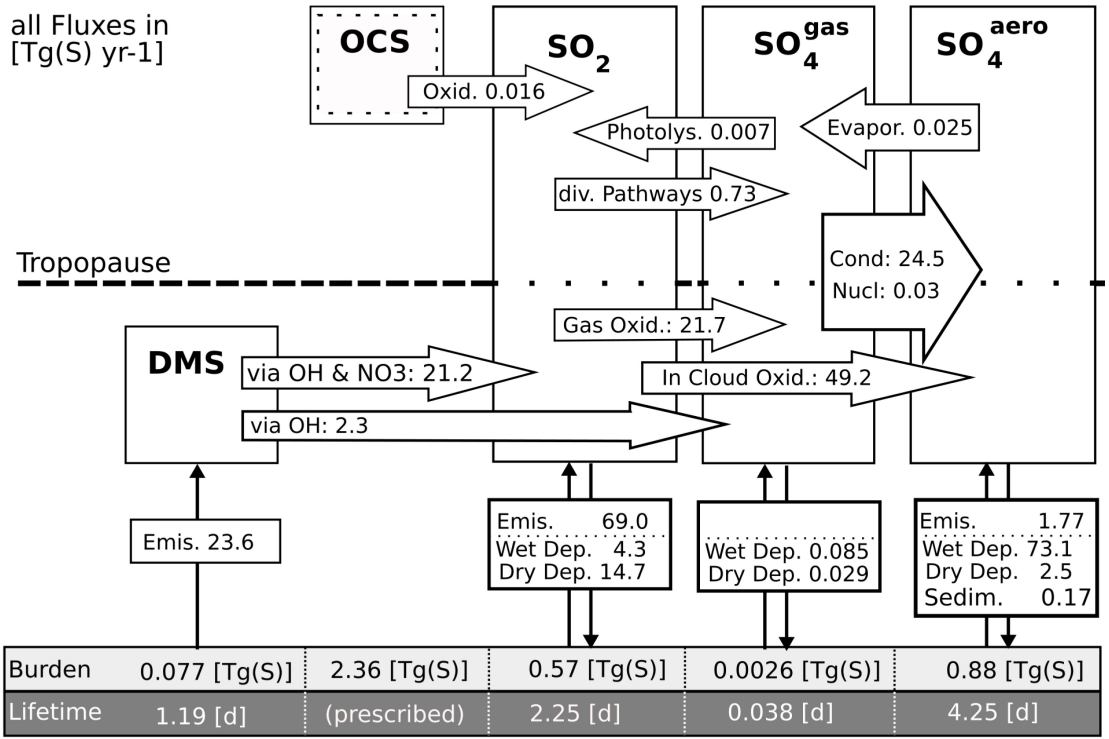

Fig. 1. Schematic budget diagnostics of model prognostic sulphur constituents in the last year of integration. All fluxes are expressed as Tg(S) y^{-1}, vertically integrated global mean column masses (burdens) as Tg(S), and whole atmosphere lifetimes as days.

GMDD
3, 1359–1421, 2010

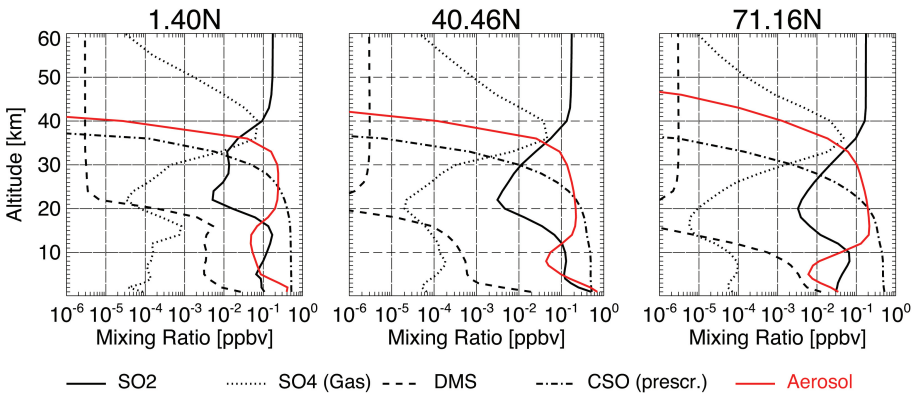

Fig. 2. Calculated vertical profiles of modelled sulphur constituents in the northern hemisphere. Shown here are climatological zonal means of the 11 year analysis period from 1996 to 2006.

GMDD
3, 1359–1421, 2010

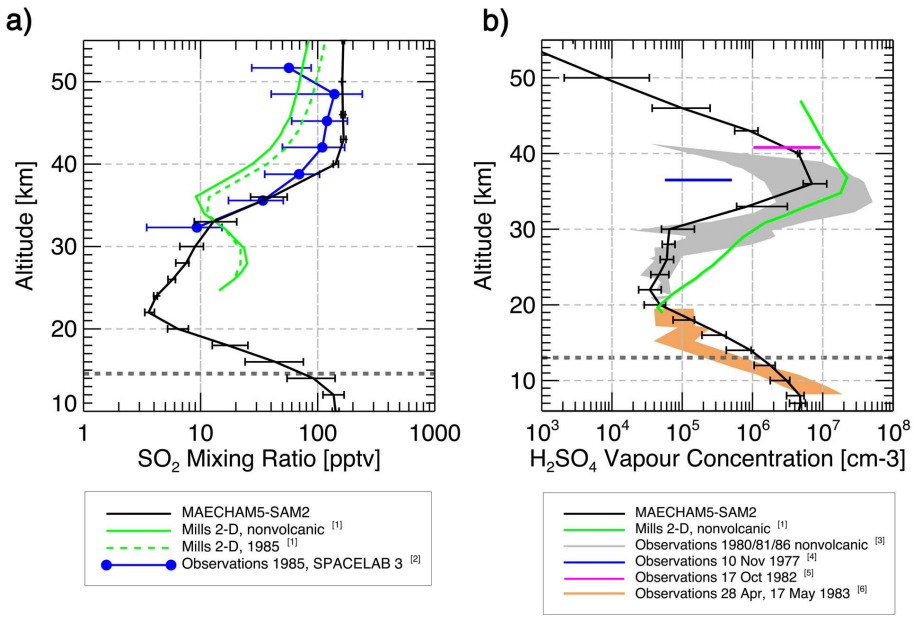

Fig. 3. Vertical profiles of modelled precursor gases in the northern hemisphere compared to results by [1] Mills et al. (2005a) and observations from [2] Rinsland et al. (1995), [3] Arnold et al. (1981), Viggiano and Arnold (1981), Schlager and Arnold (1987), and Reiner and Arnold (1997), [4] Arnold and Fabian (1980), [5] Arnold and Qiu (1984), and [6] Heitmann and Arnold (1983). [5] and [6] were conducted in the El Chichón period and [4] in a near background stratosphere prior the El Chichón eruption. For MAECHAM5-SAM2 the median of the zonally averaged climatological monthly means of the stratospheric background period 1996–2006 are shown, respective minima and maxima are represented as deviation from the median. Mills et al. (2005a) data for nonvolcanic conditions refer to years prior El Chichón. **(a)** SO_2 mixing ratio for April and May from 26 to 32° N. **(b)** H_2SO_4 vapour concentration for June, September and October at 43° N. In both figures the modelled tropopause height is marked by a dashed gray line.

GMDD
3, 1359–1421, 2010

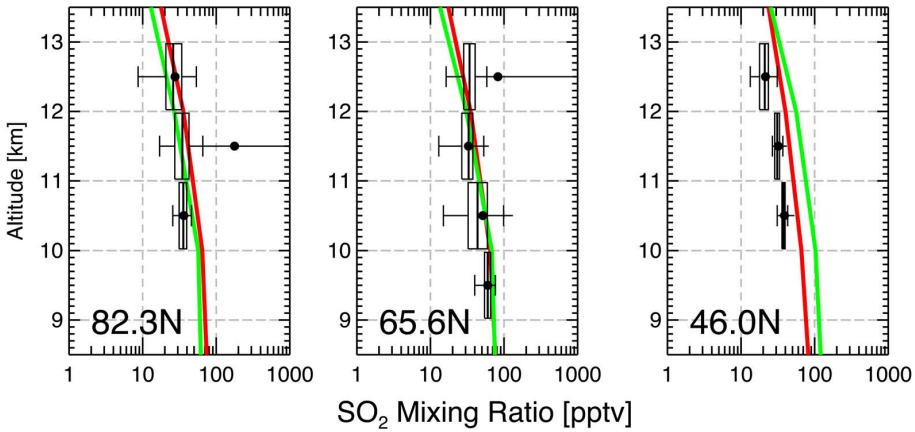

Fig. 4. Vertical profiles of modelled SO_2 at mid and high latitudes of the northern hemisphere in comparison with observational data from the NASA SOLVE campaign, conducted between December 1999 and March 2000 (Lee et al., 2003). Observations, in black, were rebinned to 1 km intervals. Shown are medians and the interquartile range (IQR), expressed as 0.25 and 0.75 percentiles, of the samples. Circles mark arithmetic mean values. The spread of the data is shown as whiskers denoting 1.5 × IRQ values, and outliers larger than that. Only measurements above the tropopause were considered. Model data are seasonal averages from 1999/2000 zonal means (DJF in red, MAM in green).

GMDD
3, 1359–1421, 2010

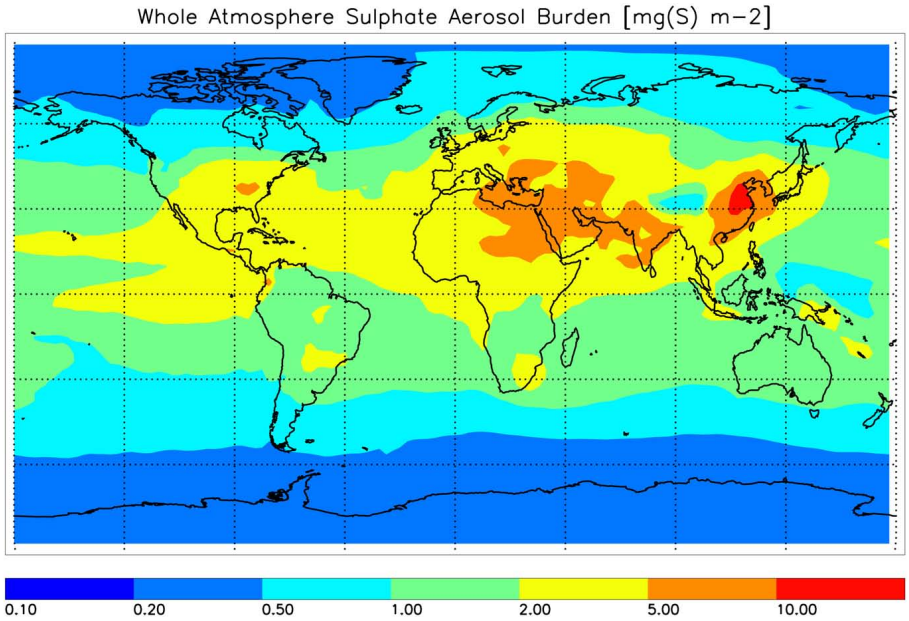

Fig. 5. Global distribution of the modelled annual mean of sulphate aerosol burden in the last year of integration.

GMDD
3, 1359–1421, 2010

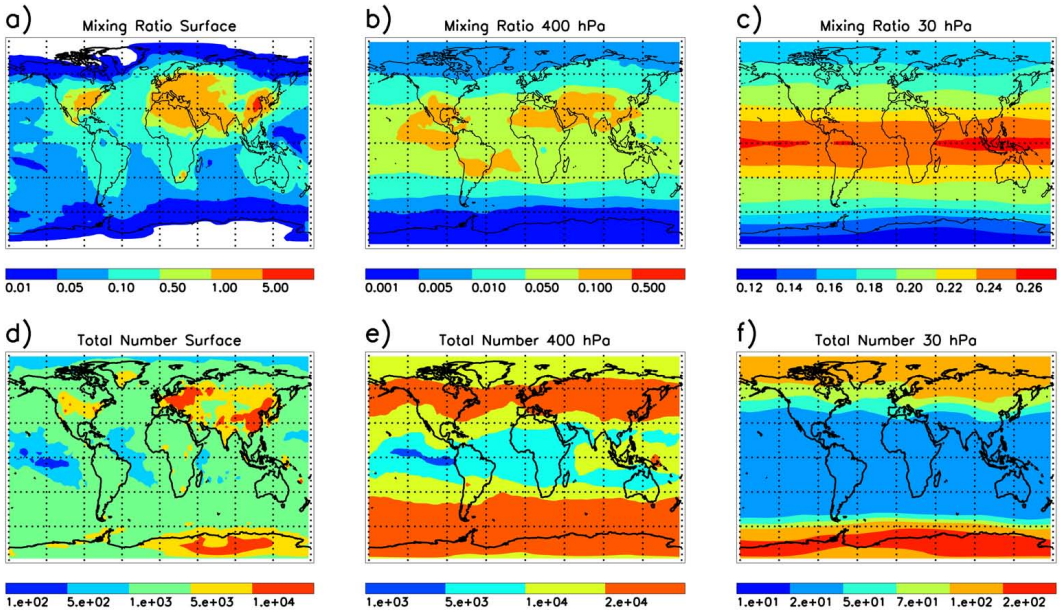

Fig. 6. Global distribution of modelled annual mean sulphate aerosol mixing ratios (top row) and total particle number concentrations (bottom row) in the last year of integration at the surface (**a** and **d**), in the free troposphere at 400 hPa (**b** and **e**), and in the stratosphere at 30 hPa (**c** and **f**). Mixing ratios are expressed as ppbm and concentrations in cm^{-3}.

GMDD
3, 1359–1421, 2010

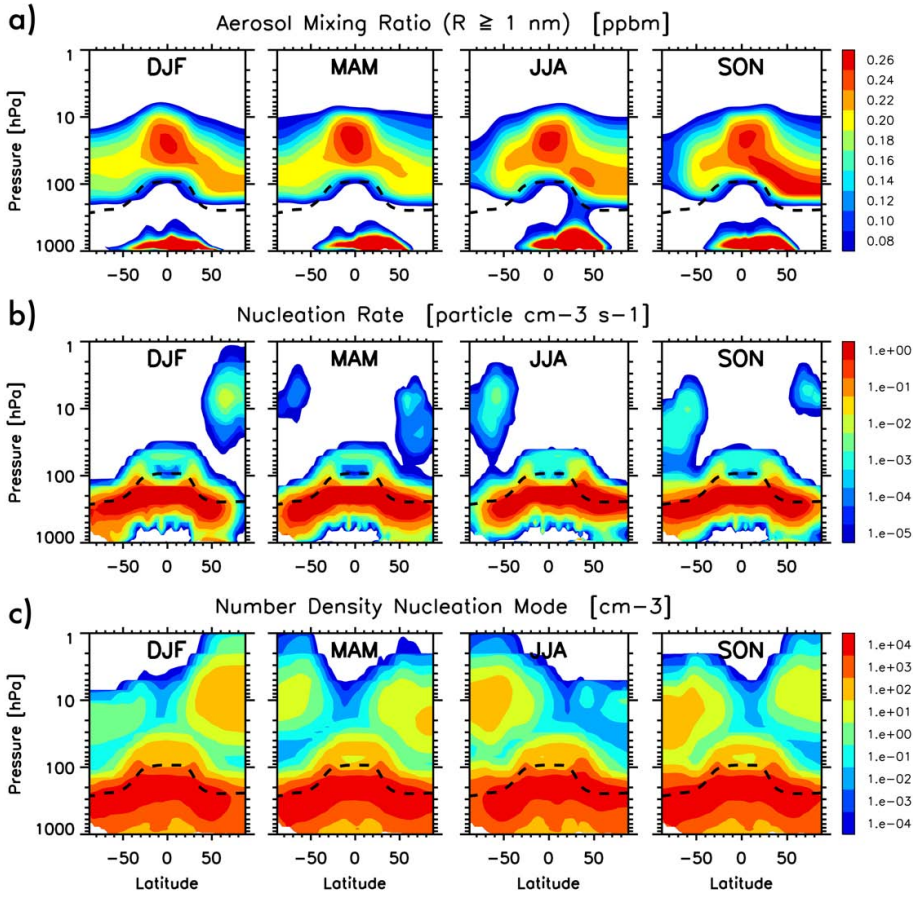

Fig. 7. Seasonal averaged climatological zonal mean **(a)** sulphate aerosol mass mixing ratio, **(b)** rate of new particle formation, and **(c)** nucleation mode number concentration.

GMDD
3, 1359–1421, 2010

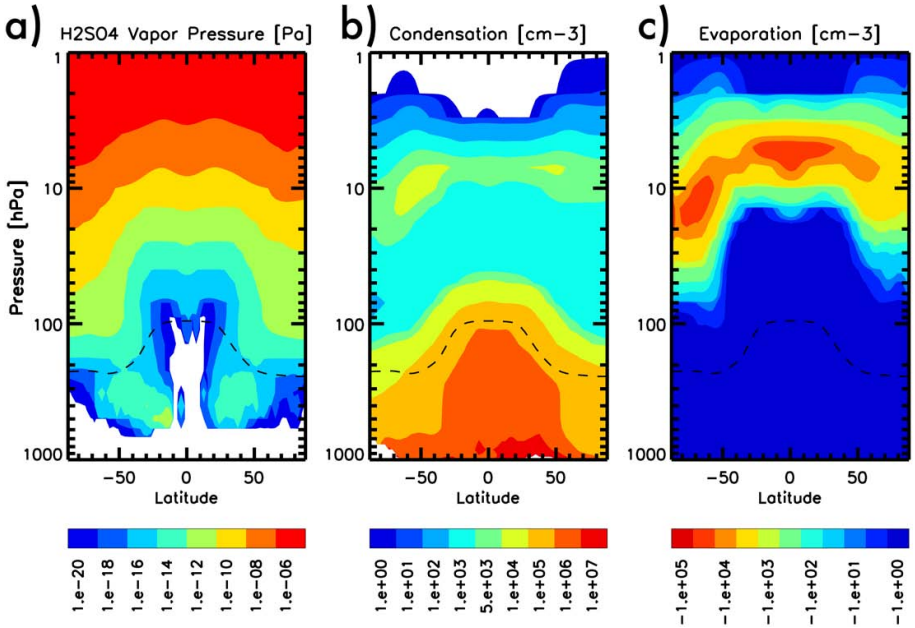

Fig. 8. Calculated climatological zonal mean **(a)** H_2SO_4 vapour pressure and the transfer concentrations of the processes **(b)** H_2SO_4 condensation and **(c)** H_2SO_4 evaporation. Note the inverted colour shading in (c).

GMDD
3, 1359–1421, 2010

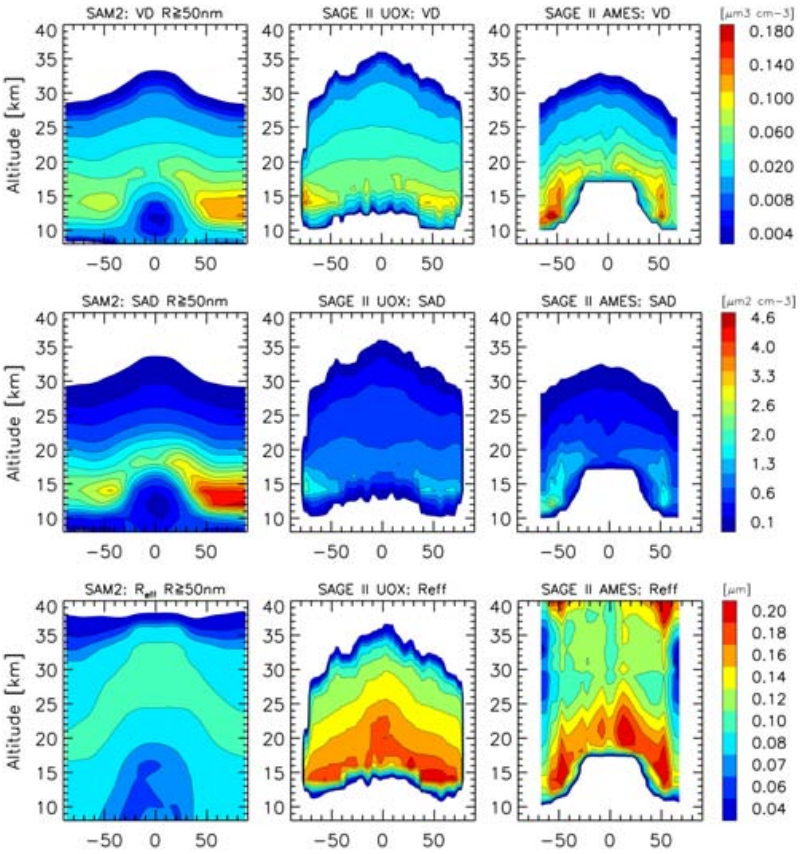

Fig. 9. Modelled climatologies (left column) of aerosol volume density (upper row), aerosol surface area density (middle row), and effective radius (bottom row), in comparison with SAGE II retrievals of the University of Oxford (Wurl et al., 2010, middle column) and NASA AMES laboratory (Bauman et al., 2003a,b, right column). All data for 1998 as zonal annual means.

GMDD
3, 1359–1421, 2010

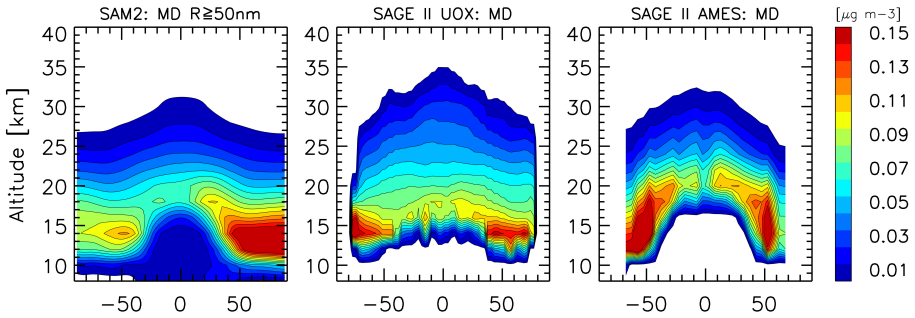

Fig. 10. As in Fig. 9, except for aerosol mass densities.

GMDD
3, 1359–1421, 2010

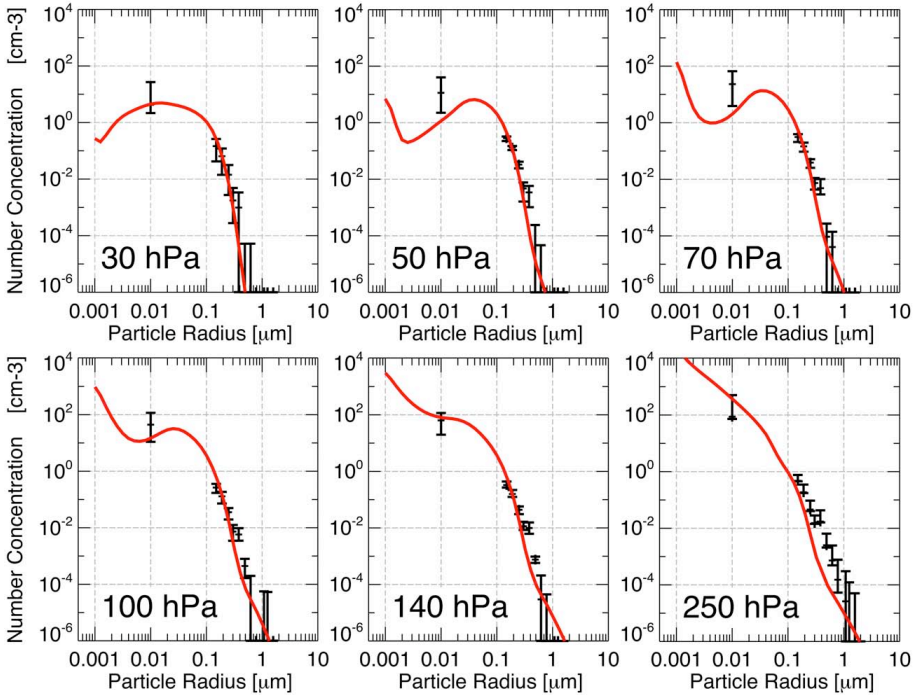

Fig. 11. Comparison of modelled size distributions with OPC measurements of particle number concentrations taken in the free troposphere and stratosphere over Laramie, WY for 2006 (Deshler et al., 2003a). Model data are represented by annual zonal means. For the OPC the median of all soundings in 2006, rebinned to the vertical resolution of the model, is shown. Whiskers denote the spread of the observations.

GMDD
3, 1359–1421, 2010

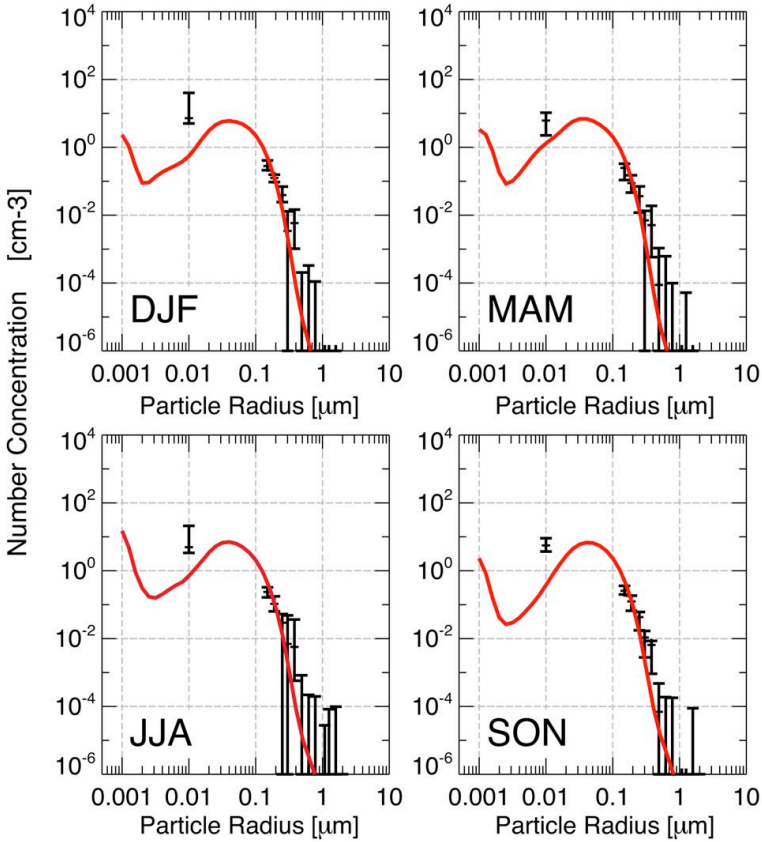

Fig. 12. Seasonal averaged aerosol size distributions in the centre of the stratospheric aerosol layer at 50 hPa over Laramie, WY. The OPC data (black) as in Fig. 11, except for the years 1998 to 2006. Model data (red) are climatological means of the grid cells corresponding to the geographical position of the station.

GMDD
3, 1359–1421, 2010

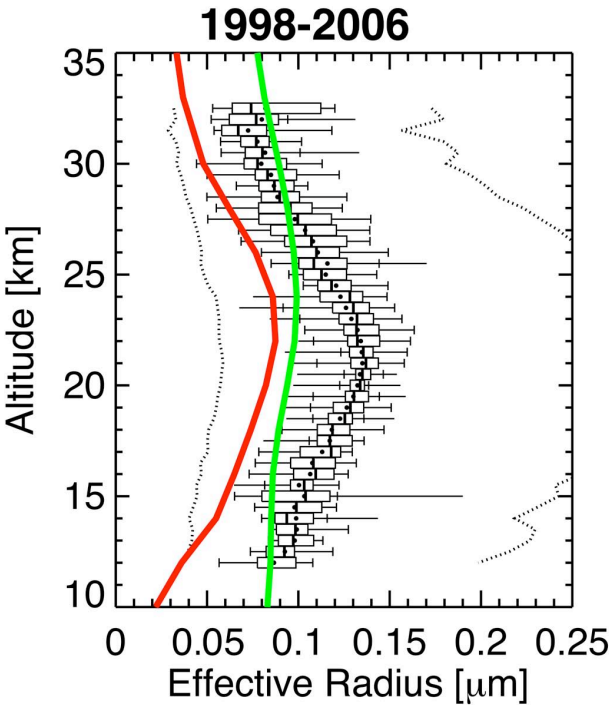

Fig. 13. Vertical profiles of the effective radius derived from OPC measurements in the stratosphere over Laramie (WY; Deshler et al., 2003a) compared to model results. The OPC data, in black, were rebinned according the vertical resolution of the model. Shown is the vertical profile of the data median. The box represents the interquartile range, i.e. 0.25 and 0.75 percentiels. Circles mark mean values of the measurements. The spread of the data is shown as whiskers denoting 1.5 × IRQ values, and outliers larger than that. Dashed lines represent R_{eff} when the error estimates of the underlying surface area and volume density integrals from size distributions fitted to measurements are taken into account, details are given in Deshler et al. (2003a). The model effective radius was retrieved for the whole spectrum ($R \leq 1$ nm; red) and for the visible range of optical instruments ($R \leq 50$ nm; green).

GMDD
3, 1359–1421, 2010